Title: Effect of Subretinal Co-Transplantation of Human Adipose-Derived Stem Cells and Derived Retinal Pigment Epithelium Cells in a Rat Model of Early and Late Age-Related Macular Degeneration

Authors: Monireh Ghasempour[1], Ali Shahbazi[2,3,*], Hamid Aboutaleb Kadkhodaian[4], Masood Naseripoor[5], Fereshteh Azedi[3]

1. *Department of Neuroscience, Faculty of Advanced Technologies in Medicine, Iran University of Medical Sciences, Tehran, Iran.*
2. *Cellular and Molecular Research Center, Iran University of Medical Sciences, Tehran, Iran.*
3. *Department of Neuroscience, Faculty of Advanced Technologies in Medical Sciences, Iran University of Medical Sciences, Tehran, Iran.*
4. *Department of Biology, Indiana University, Indianapolis, USA.*
5. *Ophthalmologist Eye Research Center, The Five Senses Health Institute, Moheb Kowsar Hospital, Iran University of Medical Sciences,Tehran, Iran.*

***Corresponding Author**: Ali Shahbazi, *Cellular and Molecular Research Center, Department of Neuroscience, Faculty of Advanced Technologies in Medical Sciences, Iran University of Medical Sciences, Tehran, Iran. Email: shahbazi.a@iums.ac.ir*

To appear in: **Basic and Clinical Neuroscience**

Received date: 2026/04/30

Revised date: 2026/07/22

Accepted date: 2026/07/27

Please cite this article as:

Ghasempour, M., Shahbazi, A., Aboutaleb Kadkhodaian, H., Naseripoor, M., Azedi, F. (In Press). Effect of Subretinal Co-Transplantation of Human Adipose-Derived Stem Cells and Derived Retinal Pigment Epithelium Cells in a Rat Model of Early and Late Age-Related Macular Degeneration. Basic and Clinical Neuroscience. Just Accepted publication Jul. 10, 2026. Doi: http://dx.doi.org/10.32598/bcn.2026.8580.1

DOI: http://dx.doi.org/10.32598/bcn.2026.8580.1

Abstract

Age-related macular degeneration (AMD) is the leading cause of blindness in the elderly. Recently, stem cells have been used to treat AMD. Here, the effect of transplantation of human adipose-derived stem cells (h-ADSCs), h-ADSC-induced retinal pigment epithelium (ADSC- iRPE), and their combination on early and late phases of AMD was investigated in rats. Labeled sub-retinal cell transplants were applied one day and two weeks after establishing retro-bulbar sodium iodate-induced AMD as early and late treatments, respectively. After 12 weeks, morphological changes in the photoreceptor and RPE layers of rat retina were assessed by measuring photoreceptor layer thickness (PLT) and outer nuclear layer row number (ONLN) in the peripheral (P), central (C), and total/average (T) regions of the retina, as well as the intensity of RPE65 protein expression (intensity). Statistical analyses of variances revealed the main effects of treatment, phase, and their interaction on PLT and ONLN (P, C, T), and the main effect of treatment on the intensity. Post-hoc analysis showed that in the early phase AMD model, PLT and ONLN (P, C) were significantly increased in all treatment groups compare to the AMD group. In addition, restoration of PLT (C) to the control-group level was observed only in the combination cell transplant group. In the late AMD model, unlike the early model, significant differences for all study variables were found between the Control group and the other groups. In conclusion, combined cell therapy in the early phase resulted in greater structural preservation of the PL in the rat model, suggesting early intervention in cellular treatments of AMD. However, the lack of functional tests should be considered when interpreting the findings of this study.

Keywords: Cell Transplantation, Mesenchymal Stem Cell Transplantation, Retinal Pigment Epithelial Cell, Age-Related Macular Degeneration

1. Introduction

Despite significant efforts and therapeutic advances, age-related macular degeneration (AMD) remains the most common cause of blindness in the elderly in developed countries (Chichagova et al., 2018, Blasiak et al., 2017). The prevalence of the disease in people over 65 years of age has been reported to be between 10% and 20% (Trincao-Marques et al., 2024). This neurodegenerative, multifactorial disease, involving the central region of the retina, gradually causes vision loss up to irreversible blindness (Chow and Mead, 2023, Pawlowska et al., 2019). In advanced stages, AMD is divided into dry (or atrophic) and wet (or neovascular) types (Deng et al., 2022). Wet AMD appears suddenly and progresses rapidly to blindness, while the dry type also progresses at a slower rate, but the final outcome is still blindness (Zhang et al., 2020). Dry AMD is more common; approximately 85% to 90% of advanced AMD cases are dry (Pinelli et al., 2020, Thomas et al., 2022).

Currently, there is no cure for patients with dry AMD (Yang et al., 2022). However, recently, stem cell-based therapy has emerged as an attractive approach to treat retinal degeneration with the potential to survive or replace degenerated cells in the retina (Lin et al., 2021, Wang et al., 2020). Several studies have investigated the potential and effectiveness of stem cells and RPE transplantation in the treatment of AMD (Chichagova et al., 2018, Deng et al., 2022, Thomas et al., 2022). Among various sources of stem cells, adipose-derived mesenchymal stem cells (ADSCs) appear to be a promising therapeutic approach due to their multiple properties and functions, such as immunoregulation, anti-apoptotic neurons, cytokine and growth factor secretion, and antioxidant activities (Adak et al., 2021). Studies have shown that ADSCs can replace dying cells, promote tissue regeneration, and support the survival and growth of retinal cells, and these cells can also differentiate into retinal and RPE cells (Finocchio et al., 2023, Lin et al., 2021, Hu et al., 2020). Furthermore, human ADSCs have the ability to survive, migrate, and differentiate into RPE cells after injection into the eye (Kadkhodaeian et al., 2018).

Since the RPE is considered a functional center for retinal homeostasis, its cellular and metabolic responses to age-related changes can be regarded as indicators of the pathogenic mechanisms that lead to the initiation and progression of AMD (Pinelli et al., 2020). In its early stages, AMD results in functional and metabolic disorders of the retina, along with the formation of drusen in the Bruch membrane beneath the RPE. In advanced stages, it leads to RPE atrophy, followed by

photoreceptor atrophy and ultimately irreversible blindness (Li et al., 2022). These disorders are linked through mechanisms involving inflammation and oxidative stress (Young et al., 2019). On the other hand, by definition, stem cell therapy involves reversing some or all of these damaged cellular changes by transplanting stem cells into the macula, paracentral retina, or intravitreal region in order to preserve or restore vision in AMD patients (Singh and MacLaren, 2018). Therefore, it seems that ADSC cells can support tissue regeneration through immunomodulatory properties and by secreting cytokines and growth factors (Finocchio et al., 2023). On the other hand, according to studies, human ADSCs prevent RPE cell death caused by oxidative stress in vitro and in vivo (Adak et al., 2021), and therefore are capable of counteracting cellular damage.

Overall, since the long-term outcomes of treating retinal degeneration with single type-cell transplantation have been reported to be poor, and perhaps combined transplantation of multiple cell types may have better long-term therapeutic results (Zhai et al., 2020, Qu et al., 2017), the hypothesis of this study is that using a combination of h-ADSC and h-ADSC-induced retinal pigment epithelium cells (ADSC-iRPE) will stop or reduce cellular damage caused by oxidative stress, followed by regeneration of damaged cells by the transplanted ADSC cells, and possible replacement of atrophic RPE cells with ADSC-iRPE cells in an AMD rat model (Chen et al., 2020). Assuming that photoreceptors are intact in the early phase of the AMD model (Chen et al., 2020), it is thought that a better therapeutic prognosis would be provided by the combined transplantation of ADSCs and ADSC-iRPE cells in Early AMD than in Late AMD. Here, the effect of transplantation of h-ADSCs, ADSC- iRPE, and their combination on early and late phases of AMD was investigated in rats. **Figure 1** summarizes and schematically illustrates rational and the possible effects of transplantation of these two cells on the damaged retinal pigment epithelium in a rat model of AMD. The selection of h-ADSC in this preclinical study was to assess beneficial effects with possible application in human studies.

2. Materials and methods

2.1. Animals

All experimental steps were performed in accordance with ARVO guidelines and ethical guidelines for working with laboratory animals approved by the Ethics Committee of Iran University of Medical Sciences. All conditions of the ethics committee were met, and the ethics code was given (ID IR.IUMS.REC.1401.135).

The study samples consisted of adult male black pigmented rats (Razi Institute/Iran/Tehran) weighing between 200 and 250 g/kg. Sixty rats were randomly divided into 10 equal groups (6 rats per study group, Table 1): five groups for the early AMD model and five groups for the late AMD model. Rats received retrobulbar injections of sodium iodide to induce the AMD model in one eye (randomly half of the rats received the injection in the right eye, and the other half in the left eye) whereas the control groups received PBS accordingly. Sodium iodide first damages RPE cells and then the neuroretina, leading to complete visual impairment within two weeks (Chen et al., 2020). Because retinal cells undergo apoptosis one day after sodium iodide injection (Hu et al., 2020), the early AMD groups received labeled cells or PBS subretinal transplantation in the study eye 24 hours after sodium iodide injection to possibly inhibit retinal cell apoptosis. In contrast, the Late AMD groups received labeled cells or PBS two weeks after injection. Given that sodium iodide is metabolized within minutes in the body (Hu et al., 2020), the transplanted cells will not be damaged by sodium iodide after subretinal injection. At 12 weeks after transplantation, all animals in the groups were euthanized, and then the studied eyes were enucleated to assess the therapeutic effects. Rats were maintained under standard laboratory conditions with a 12-hour light/dark cycle at 20-24°C. **Figure 2** schematically illustrates the study phases and design.

2.2. Isolation and culture of human adipose stem cells

This step was performed based on the study by Zhang et al. with a slight modification (Zhang et al., 2017). In short, fat tissues of individuals between 25 and 35 years old were washed several times, cleaned of vessels and stains, finely chopped with surgical scissors, and added to a 1:1 collagenase type 1 (collagenase type 1 lyophilized (17100-017, Gibco, USA)) solution,. The mixture was placed in the incubator for 75 min, and then centrifuged twice for 5 min at 1200 rpm. After filtering, it was centrifuged again. Finally, complete D-MEM culture medium [D-MEM (Dulbecco's Modified Eagle Medium (D-MEM; 12800-082, Gibco, USA)), 1% penicillin-streptomycin (Penicillin-Streptomycin (PS; p06-07100, BIOTECH, USA)), 10% FBS (Fetal Bovine Serum (FBS; FB-1001/100, Biosera, France)), and 2% amphotericin B (15290026, Gibco UK)] was added to the settled cells, and the cells were transferred to an incubator with 5% CO2. The medium was changed every two days until the cells reached 85%-90% confluence. Cell viability and quantity were measured at each passage.

2.3. Confirmation of the identity of adipose tissue-derived stem cells by immunocytochemistry

In this study, two markers, CD73 and CD90 were used by immunocytochemistry (ICC) to demonstrate the identity of h-ADSCs. This step was performed based on the study by Kadkhodaeian et al., with slight modifications (Kadkhodaeian et al., 2019). Briefly, passage 4 h-ADSCs were washed with PBS (Phosphate-Buffered Saline (PBS; 18912-014, Gibco, UK)), fixed in 4% paraformaldehyde (Art-Nr.0335.2, Roth, US), incubated in 0.25% Triton x-100 (BP151-500, Fisher, UK) for 15 minutes, washed with PBS, and placed in blocking solution (1% BSA; (Bovine Serum Albumin, BSA; A9647, Sigma-Aldrich, US)). Primary antibodies, CD73 (Monoclonal Antibody (7G2), Product no#41-0200, Thermofisher, USA) and CD90 (Monoclonal Antibody (F15-42-1) 200µg, Product no#MA5-16671, Thermofisher, USA), were used at concentrations of 1:25 and 1:50, respectively, in diluted blocking solution (0.2% BSA) for positive reactions and without antibody for negative reactions, and were incubated overnight at 4°C. After washing the antibodies with the solution (0.1% Tween 20 (8.22184.0500, Sigma-Aldrich, France) + PBS), the secondary antibody—goat anti-mouse IgG (H+L), super clonal™ recombinant secondary antibody (A28175, Thermo Fisher, USA)—diluted at 1:500, was used and incubated for 1 hour at room temperature. Finally, cells were incubated in DAPI (Alexa Fluor™ 488 Dapi (D9542-1MG, Sigma-Aldrich, Israel)), and were observed and imaged with an Olympus inverted fluorescent microscope.

2.4. Differentiation of human adipose stem cells into retinal pigment epithelial cells

Differentiation of h-ADSCs into RPE-like cells was performed indirectly according to two studies by Aboutaleb et al. and Yang et al., with modifications (Aboutaleb Kadkhodaeian et al., 2019, Yang et al., 2015). First, h-ADSCs were differentiated into neurospheres, then neural stem cells (NSCs), and finally into RPE-like cells. The 4th passage h-ADSCs were used for differentiation into neurospheres. Complete neurosphere medium (DMEM/F12 (D-MEM/F12 + GlutaMAXTM 1x (10565-018, Gibco, UK)), 20 ng/mL b-FGF (Recombinant Human FGF-basic ((154 aa) (Animal-Free), Bio Legend, USA)), 20 ng/mL EGF (Human EGF (AF-100-15-100UG, Peprotech)), 2% B27 supplement (50x) (17504-044, Gibco, USA), 1% penicillin/streptomycin) was added to non-treated 6-well plates containing the cells. The cells were maintained in an incubator with 5% CO2. On days 10 to 12, the neurospheres were fully formed and had increased in size. At this stage, the

cells were placed in DMEM/F12 basal medium with 1% N2 supplement ((100x) (17502-048, Gibco, USA)) for 48 hours. Then, cells were passaged to produce and propagate neurospheres. The third passage neurospheres were used to differentiate NSCs. Complete neural stem cell medium (complete neurosphere medium + 1% FBS) was added into a 6-well plate containing these cells. After 10 to 12 days, the cells were passaged.

The third passage NSCs were used to differentiate into RPE-like cells. NSCs at passage 3 were seeded into complete NSC medium for 10 days; then, the medium was removed and exchanged with freshly prepared RPE differentiation medium (D-MEM, 1% P/S, 1% FBS, 2 mM GlutaMAX^{TM} 100x (35050-038, Gibco, UK), 0.01 nM T3 hormone (3,3',5-triiodo-L-thyronine (T3; T6397, Sigma-Alderich, USA)), 2.4 µM putrescine dihydrochloride (P5780, Sigma-Aldrich, Switzerland), 0.063 µM transferrin human (T3309, Sigma-Aldrich, USA), 0.83 µM insulin solution human (I9278, Sigma-Aldrich, USA), 0.3µM linoleic Acid-Water Soluble (L5900, Sigma-Aldrich, USA), 0.028 µM hydrocortisone (H0888, Sigma-Aldrich, USA), 0.014 µM selenous acid (211176, Sigma-Aldrich, USA)) to induce RPE-like cells. The medium was changed two to three times a week. Cells were collected for ICC on day 18 at approximately 60% confluence, when they were fully transformed and pigmented. Cells were passaged on day 27 at 80%–85% confluence. For further proliferation and growth, the cells were recultured after the first passage. In each passage, cell viability and quantity were measured.

2.4. Immunocytochemistry of differentiated RPE cells

Differentiated RPE cells were examined using the ICC analysis proposed by Kadkhodaeian et al. for the designated marker (Kadkhodaeian et al., 2019). Differentiated RPE cells derived from NSCs were stained before the first passage and the second passage. Briefly, cells were washed with PBS and fixed in 4% paraformaldehyde, incubated in Triton 100x (0.25%) for 15 minutes, blocked for 1 hour at room temperature with blocking solution (1% BSA). Then, for one well, the primary antibody RPE65 (anti-retinal pigment epithelium 65 antibody (MAB5428, Sigma, US)) was added at a concentration of 1:50 in diluted blocking solution (0.2%), and for the other well, only the diluted blocking solution was added for negative reaction testing. The cells were incubated in the refrigerator overnight. After washing with the primary antibody (washing solution: 1% Tween20 plus PBS), they were incubated with the secondary antibody, goat anti-mouse IgG, at a concentration of 1:500 for 1 hour at room temperature. The cells were then incubated in DAPI

(3µg/ml) for 5 minutes, and finally observed and imaged with an Olympus inverted fluorescent microscope; All ICC and IHC images were captured using Mosaic V2.4 software by a camera attached to an Olympus inverted fluorescent microscope made in the Philippines.

2-5. Retinal degeneration model induction in rats

Sodium Iodate ((NaIO3), a stable oxidizing agent, can selectively damage RPE cells, convert glycine to potentially toxic glyoxylate in melanocytes of RPE cells, and also inhibit the activity of some enzymes in RPE cells. This NaIO3-induced retinochoroidal degeneration is used as an animal model of dry AMD (Moriguchi et al., 2018).

Hanus et al. showed that after the AMD model was established by retro-bulbar injection of NAIO3 at a dose of 20 mg/kg, RPE cells appeared PI positive after 24 hours of NaIO3 injection (Hanus et al., 2016). Also, a study showed that intravenous injection of 25 mg/kg of NaIO3 first damages the RPE and then affects the retina, and after two weeks, complete vision is lost (Chen et al., 2020). In this study, the model was created with a dose of 25 mg/kg sodium iodate (S4007-100G Sigma-Aldrich, Germany) as a retrobulbar injection. According to the study by Yardeni et al., a 30-gauge, 12-mm insulin syringe and an injection volume of 150 µL were used for retrobulbar injection (Yardeni et al., 2011). Before sodium iodide injection, the animals were first anesthetized with an intraperitoneal injection of ketamine 100 mg/kg and xylazine 10 mg/kg. The cornea was numbed by instilling 0.5% tetracaine eye drops (Sina-Daru/Iran). The animal was then placed laterally under the surgical microscope. The needle was inserted into the medial canthus. After the injection was completed, the needle was gently withdrawn. The injection was confirmed by eye protrusion. Finally, eye drops were used to reduce the risk of infection.

2.6. Transplantation of h-ADSC, ADSC-iRPE, and their combined cells into the subretinal space

Basically, there are three routs of subretinal injection: (1) Transcorneal route; (2) Anterior transscleral route; and (3) Posterior transscleral route (Parikh et al., 2016, Irigoyen et al., 2022). In this study, the third method of subretinal injection was used.

Groups E.AMD, E.AMD+h-ADSC, E.AMD+RPE, and E.AMD+h-ADSC+RPE, were prepared to receive PBS/or the relevant transplantation of cells labeled with CM-DiI (CellTracker TM CM-DiI (C7000, Invitrogen, US) 24 hours after NaIO3 injection. Groups L.AMD, L.AMD+h-ADSC,

L.AMD+RPE, and E.AMD+h-ADSC+RPE received PBS or the relevant transplantation of cells two weeks after NaIO3 injection. Mixed cells (5 µL, 5×10^5 cells; half h-ADSCs and half ADSC-iRPE cells), ADSC-iRPE cells (5 µL, 5×10^5 cells), h-ADSCs (5 µL, 5×10^5 cells), and PBS (5 µL, 0.001 M) were injected subretinally according to the study by Parikh et al. (Parikh et al., 2016). (Parikh et al., 2016).

Briefly, after intraperitoneal injection of ketamine 100 mg/kg and xylazine 10 mg/kg (for anesthesia), 2.5% phenylephrine and 0.5% tetracaine eye drops were instilled into the eyes to dilate the pupils and numb the cornea. The animal was placed laterally under the surgical microscope. The injection site was identified in the posterior pole of the eyeball, in the conjunctiva, using a 27-gauge needle. A Hamilton needle (30 gauge) was used to pass through the conjunctiva, sclera, and choroid into the subretinal space, and 5 µl of the desired suspension was injected. At the same time, a small hole was made in the outer edge of the cornea to prevent an increase in intraocular pressure. The injection was confirmed by observing the fundus under a microscope and a bulge or bleb. Eye drops were used to reduce the risk of infection and corneal damage.

2.7. Tissue preparation and immunohistochemistry

All specimens were euthanized after 12 weeks of subretinal graft injection under anesthesia. The tissue preparation method was based on the study by Geathers et al., with a slight modification (Geathers et al., 2024). To perform the fixation procedure, the eyes of the samples were washed twice with PBS after enucleation, placed in Falcon tubes containing 4% paraformaldehyde, and incubated in the refrigerator overnight. After fixation, tissue processing and paraffin embedding were performed for all study samples.

To investigate changes in retinal tissue structure, three types of tests were performed: testing morphological changes in retinal tissue, testing protection, regeneration, and replacement of transplanted cells, and testing the therapeutic effects of transplanted cells on RPE damaged by sodium iodide.

2.7.1. Assessment of morphological changes in retinal tissue

Tissue sections for structural evaluation of retinal tissue are usually prepared from 100 µm of the optic disc and 500 µm of the Ura Serata (Enzmann et al., 2006, Kadkhodaeian et al., 2016). In this study, cross-sectional sections from these two regions were prepared from 4 out of 6 samples from

each of the two AMD model groups. Sections from the remaining two samples from each group were used for the other two tests of the study. For morphological analysis of retinal tissue, i.e., measuring the outer nuclear layer rows number (ONLN) and the thickness of the photoreceptor layer (PLT), 7 µm sections were prepared at two locations: (1) approximately 100 µm from the optic nerve head and (2) approximately 500 µm from the Ura Serrata (the border of the ciliary body and retina). After dewaxing, the sections were stained with hematoxylin and eosin (H&E) and counting was performed on the images (Geathers et al., 2024). For each sample from each location, 4 images were prepared from different points (4 central images and 4 peripheral images), and the data were quantified using ImageJ software. This average was recorded as the data for the central and peripheral parts of the retina for one sample separately. Thus, for each sample, one quantitative value for the central part, one for the peripheral part, and one for the entire retina (the average of the central and peripheral parts) were used separately for analysis. To prevent bias in the selection of images, a person unaware of the research objectives and retinal structure was used. All H&E images were captured using Mosaic 2.4 software by a camera attached to an LaboMED Lx300 microscope (USA).

2.7.2. Labeling and Track of Transplanted cells

To determine the fate of the transplanted cells, according to the study by Kadkhodaeian et al., the transplanted cells were labeled before subretinal injection (Kadkhodaeian et al., 2018). To label and track ADSCs from passage 4 and differentiated RPE from passage 2 after cell confirmation, the fluorescent marker CM-DiI was used according to the study by Linghui et al. (Qu et al., 2017).

2.7.3. Measurement of fluorescence intensity of RPE layer (RPE65)

To investigate the therapeutic effects of single type-cell or combined transplantation on RPE damaged by sodium iodide, based on the study by Barzelay et al., the RPE65 antibody was used (Barzelay et al., 2018). The sections were stained according to the protocol of Zaqout et al. (Zaqout et al., 2020). Paraffin-embedded ocular tissues with 7 µm sections mounted on high-adhesion positively charged slides were prepared for staining after drying. Briefly, after dewaxing, unmasking, permeabilization, and blocking, the primary antibody RPE65 (anti-retinal pigment epithelium 65 antibody (MAB5428, Sigma, US)) was used at a concentration of 1:50 and stored in the refrigerator overnight. After washing with PBS, the sections were placed in a PBS/Gelatin/Triton20 solution and incubated for one hour with a secondary antibody, goat anti-

mouse IgG (1:500), at room temperature. They were then washed with PBS and placed in a solution of 10 mM CuSO4 and 50 mM NH4CL for ten minutes. This solution reduces lipofuscin-like autofluorescence. Lipofuscin can interfere with the detection of IF signals (Zaqout et al., 2020). After staining by DAPI (3 µg/ml), samples were observed and imaged with an Olympus inverted fluorescent microscope. ImageJ software was used to evaluate the fluorescence intensity of the RPE layer

2.8. Statistical Analysis Method

Normality of the data was tested using the Shapiro-Wilk test (data were normally distributed). Two-way ANOVA was also used to compare the means of variables between the early and late AMD models; this was followed by comparisons of variables between groups of both Early and Late AMD models using separate one-way ANOVA tests followed by Tukey's test. All data were presented as mean ± standard deviation (SD). P-values less than 0.05 were considered statistically significant. SPSS software was used to analyze the data.

3. Result

3.1. Extraction and culture of human adipose tissue-derived stem cells

Primary culture cell passage was performed after seven days. **Figure 3**A-D shows human adipose tissue-derived stem cells at different passages. After each passage, the cells were qualitatively and quantitatively assessed with Neobar slides and Trypan Blue. Cell viability was between 95% and 98% at different passages.

3.2. Confirmation of the identity of adipose-derived stem cells by immunocytochemistry

To identify the identity of h-ADSCs, two markers, CD73 and CD90, were used by ICC. This test showed a positive reaction for both markers. **Figure 4** A and B shows images taken with an Olympus inverted fluorescent microscope with the two markers, CD90 and CD73, respectively. Images of the negative reaction are not shown.

3.3. Differentiation of human adipose-derived stem cells to retinal pigment epithelium cells

As previously mentioned, the differentiation of h-ADSCs into RPE-like cells was indirect; they first differentiated into neurospheres (neural progenitor cells), then into neural stem cells (NSC), and finally into RPE-like cells.

First, fourth-passage ADSCs were used for differentiation into neurospheres. **Figure 5**A-D shows the stages of neurosphere formation, where the cells become clonal and gradually change shape; in the final stages of their growth, they become round in shape with spikes attached all around their periphery. Then, the third passage neurospheres were used to differentiate into NSCs. **Figure 6**A-F shows the stages of differentiation of NSCs, showing how the appearance of the cells changes from spherical to cone-shaped and fibroblast-like. Finally, passage 3 NSCs were used for RPE differentiation. The changes in NSCs during differentiation into RPE can be seen in **Figure 7**A-F. The cells from the first passage were re-cultured for further growth and proliferation. As shown in **Figure 8**A-B, RPE-like cells show differentiation from NSCs derived from h-ADSC. The cells became almost homogeneous and were similar to RPE cells. These changes can also be seen in ICC staining.

3.4. Immunocytochemistry of RPE cells differentiated from h-ADSCs

As mentioned previously, NSC-derived RPE cells differentiated from h-ADSCs were stained with the RPE65 marker before the first and second cell passages. Based on the stained images, the positive reaction of these cells to the RPE65 marker appears to be different at the two cell passages (**Figure 9**A and B). The staining level (indicating the level of RPE65 protein expression by RPE cells) appears to be much higher and more consistent before the second cell passage than the first cell passage.

3.5. Retinal tissue imaging

3.5.1. Morphological changes in retinal tissue

Histological alterations in peripheral and central areas of the retina in different studied groups are shown in **Figure 10** A and B. In the E.AMD and L.AMD groups, a decrease in the thickness of the retinal layers and disruption of the cellular structure were observed compared to the E.Control and L.Control groups. Apparently, the layered structure and relative retinal thickness in the treatment groups in the early AMD model were preserved similar to the E.Control; however, in the late AMD model, relative preservation of the layered structure and increased retinal thickness were observed compared to the L.AMD groups.

The mean photoreceptor layer thickness (PL.T) and the outer nuclear layer rows number (ONL.N) in the three regions of the peripheral (P), central (C), and the whole retina (T: average of peripheral

and central) among the five groups of the early AMD and late AMD models are presented in Tables 2 and 3. Two-way ANOVA was used to examine the main effect of early and late phases of AMD, AMD, the effect of treatment (groups), and their interaction on the different variables.

The results of two-way ANOVA for the variables PL.T(P)), PL.T(C), PL.T(T) and ONL.N(P), ONL.N(C), ONL.N(T) (**Figure 11**A-F) showed that the main effect of the phase on these variables was significant ($p \leq 0.001$): PL.T(P)= [$F(1,30)=32.521$, $P<0.001$], PL.T(C)= [$F(1,30)=22.533$, $P<0.001$], PL.T(T)= [$F(1,30)=40.296$, $P<0.001$], ONL.N(P)= [$F(1,30)=46.930$, $P<0.001$], ONL.N(C)= [$F(1,30)=21.655$, $P<0.001$], and ONL.N(T)= [$F(1,30)=49.900$, $P<0.001$], indicating that the mean of each variables was significantly different between the early and late AMD models. The mean photoreceptor thickness and the outer nuclear layer rows number were significantly higher in the early than in the late AMD models. The main effect of treatment was significant ($P<0.001$): PL.T(P)= [$F(4,30)=34.334$, $P<0.001$] , PL.T(C)= [$F(4,30)=59.159$, $P<0.001$] , PL.T(T)= [$F(4,30)=74.295$, $P<0.001$] , ONL.N(P)= [$F(4,30)=32.007$, $P<0.001$], ONL.N(C)= [$F(4,30)=58.721$, $P<0.001$] , and ONL.N(T)= [$F(4,30)=71.011$, $P<0.001$], indicating that the type of treatment had an effect on the amount of each variable. In addition, the interaction effect of phase×treatment was also significant ($P<0.001$): PL.T(P)= [$F(4,30)=8.103$, $P<0.001$], PL.T(C)= [$F(4,30)=4.191$, $P<0.001$], PL.T(T)= [$F(4,30)=8.000$, $P<0.001$], ONL.N(P)= [$F(4,30)=7.440$, $P<0.001$] ONL.N(C)= [$F(4,30)=5.846$, $P \leq 0.001$] , and ONL.N(T)= [$F(4,30)=9.876$, $P<0.001$].

To compare the mean of the variables between groups in both the early and late AMD models, one-way ANOVA was performed followed by Tukey's test. There was a significant difference between the mean of the relevant variables among the groups in the early AMD model: PL.T(P)= [$F(4,4)=13.197$, $P<0.001$], PL.T(C)= [$F(4,4)=20.317$, $P<0.001$], PL.T(T)= [$F(4,4)= 26.628$, $P<0.001$], ONL.N(P)= [$F(4,4)= 36.550$, $P<0.001$], ONL.N©= [$F(4,4)= 32.683$, $P<0.001$], ONL.N(T)= [$F(4,4)= 43.540$, $P<0.001$]; and the Late AMD model: PL.T(P)= [$F(4,4)= 46.171$, $P<0.001$], PL.T(C)= [$F(4,4)= 72.697$, $P<0.001$], PL.T(T)= [$F(4,4)= 82.055$, $P<0.001$], ONL.N(P)= [$F(4,4)= 13.011$, $P<0.001$], ONL.N©= [$F(4,4)= 31.926$, $P<0.001$], ONL.N(T)= [$F(4,4)= 37.823$, $P<0.001$]. In the early AMD model, there was a different pattern in the Early model's treatment responses to PL.T and ONL.N in the peripheral and central parts of the retina. In the peripheral part, there was a significant difference between the AMD group and the other groups. In the central part, except for this case ($p<0.01$), there was a significant difference between the control group

and the two E.AMD+RPE and E.AMD+h-ADSC groups ($p<0.01$). For the mean PL.T and ONL.N of the whole retina, the statistical results were almost similar to the central part. In the Late AMD model, there was a significant difference between the mean of PL.T (P, C) and ONL.N (P, C) in the L.Control group compared with the other groups ($P\leq0.001$).

3.5.2. Protection, regeneration, and replacement of transplanted cells

To track the location and fate of transplanted cells, h-ADSC and ADSC-iRPE cells were labeled with a fluorescent dye (red dye, CM-DiI) before transplantation. The presence of these cells in the vicinity of degenerated areas indicates their ability to migrate purposefully to the damaged area. The distribution of the cells in the photoreceptor and inner layers of the retina indicates their tendency to replace lost cells and establish structural connections with the host tissue **(Figure 12)**. In addition, less tissue destruction was observed in areas where transplanted cells were present, which could support the protective role and reparative effects of transplanted cells against damage caused by the AMD model.

3-5-3. Therapeutic effects of transplanted cells on RPE damaged by sodium iodide

The RPE65 antibody was used to evaluate the therapeutic effects of transplanted combined and single-type cells on RPE damaged by sodium iodide. In order to control and reduce the autofluorescence of the RPE layer, after the application of secondary antibody, the slides were placed in a solution of 10 mM CuSO4 and 50 mM NH4CL for 10 minutes. Lipofuscin can interfere with the detection of IF signals. IHC alterations in the expression of RPE65 protein in different studied groups are shown in **Figure 13**. In the control groups, RPE65 expression was observed almost regularly in the RPE layer compared with the other groups. However, the staining intensity in the AMD groups was minimal. In other words, the expression intensity of RPE65 in the treatment groups, especially E.AMD+h-ADSC+RPE, showed a relative increase compared with the AMD groups.

The mean of the intensity of RPE65 protein expression (intensity) between the 5 groups of early AMD and late AMD models is presented in **Tables 2** and **3**. According to these tables, in each model, the highest mean belonged to the control groups and the lowest to the AMD groups.

The results of the two-way ANOVA showed that the effect of treatment groups on intensity was significant (intensity= ($F(4,30) =21.61$, $P<0.001$), indicating a statistically significant difference

between different treatment levels. In contrast, the main effect of group and the interaction effect of phase×treatment on intensity were not significant (P>0.05; **Figure 14).**

Based on the results of one-way ANOVA, the mean intensity was significantly different between the groups in both models (early and late), respectively([F (4,4) =10.81, p<0.001)] and [F (4,4) =11.25, p<0.001]). These results indicate that the types of treatment groups had an effect on the intensity of RPE65 expression. Tukey's post hoc test results showed that in the early AMD model, there was a significant difference between the mean intensity of the E.Control group and the other groups except E.AMD+h-ADSC+RPE (P<0.01), as well as between the E.AMD group and the E.AMD+h-ADSC+RPE group. However, no statistically significant difference was observed between the other groups. In the late AMD model, the difference in the mean intensity was significant between the L.Control group and the other groups (P<0.05), while there was no statistical difference between the other groups.

4. Discussion

In the first phase of this study, h-ADSCs were extracted and indirectly differentiated into RPE-like cells, confirmed using a specific marker for RPE cells (RPE65). These findings are consistent with previous studies that have demonstrated the efficacy of similar methods in differentiating stem cells into RPE cells (AboutalebKadkhodaeian et al., 2021, Zhang et al., 2017, Zhu et al., 2022). In the second phase, h-ADSCs, ADSC-iRPE, and their combined cells were subretinally transplanted in rat models of AMD, and structural indices of the retina were examined. The graft cells were able to restore part of the function of the damaged tissue and produce favorable changes in the repair indices. In numerous studies, the therapeutic outcomes of various stem cells have been investigated in separate or combined ways (Sharma and Jaganathan, 2021, Holan et al., 2021, Qu et al., 2017). However, to our knowledge, the evaluation of the combined cells (h-ADSCs+ADSC-iRPE), as well as the comparison of the results of simultaneous cell therapy between the two AMD models with cell transplantation 24 hours and two weeks after model creation by sodium iodide in the peripheral and central parts of the retina, have not been studied. The results revealed that the means of all variables were different between the Early AMD and Late AMD model groups; the highest means were observed in the control groups and the lowest in the AMD groups.

Also, analysis of variance showed the main effects of treatment, phase, and their interaction on PLT and ONLN (P, C, T) (p<0.001). These results are consistent with most studies that have

investigated different treatment effects in early or late AMD models or regardless of disease stage (Finocchio et al., 2023, Diniz et al., 2013, Zhu et al., 2022, Adak et al., 2021). The post hoc Tukey's test results showed a different pattern in the treatment responses of the early AMD model to PLT and ONLN in the peripheral and central retina. In the peripheral part, a significant difference was observed between the E.AMD group and the other groups ($p \leq 0.001$). In the central part, except for this case ($p < 0.01$), a significant difference was observed between the E.Control group and the two groups of E.AMD + RPE and E.AMD + h-ADSC ($p < 0.01$).

In the late AMD model, unlike the early model, a significant difference was observed between the L.Control group and the other groups ($P \leq 0.001$). For the PLT (P), there was also a significant difference between the L.AMD and L.AMD + ADSC + RPE groups ($P \leq 0.001$), and for PLT (C) among the L.AMD group and the two groups of L.AMD + ADSC + RPE and L.AMD + ADSC. These findings indicate that in the early model, assuming a healthy neuroretina, the effectiveness of stem cell-based therapy was greater, especially in the peripheral part of the retina, where RPE cells showed minimal damage at the time of transplantation. None of the three treatment groups showed significant differences with the control group, which also indicates the graft combined cells effect compared to the effect of these cells separately. This finding is consistent with previous studies that have examined the combined effects of two or more cells (Qu et al., 2017, Zhai et al., 2020).

In histological part, graft cells were identified in different layers of the retina, as in the previous study (Kadkhodaeian et al., 2018). The presence of these cells in the vicinity of degenerated areas indicates their ability to migrate purposefully to the damaged area. This finding indicates that, in addition to their ability to integrate into retinal tissue, transplanted cells may also play a role in maintaining the function of the remaining cells through the secretion of neurotrophic factors or paracrine effects (Finocchio et al., 2023).

In the results of the immunohistochemical section of the study, RPE65 expression was observed almost regularly in the RPE layer in the control groups, but a significant change in the intensity of staining was observed in the AMD groups compared to the other groups, indicating a disruption in the expression of RPE65 in response to retinal damage. Among the treatment groups, the E.AMD+h-ADSC+RPE group had a significantly higher staining intensity than the E.AMD group. Also, the results showed that only the effect of treatment group on the intensity of protein

expression was significant (P<0.001); the main effect of the model and the interaction effect of phase×treatment were not significant. Based on these findings, it seems that the type of treatment has a significant effect on intensity. However, this effect is not dependent on the type of model (early or late) and the changes in both models show a relative similar pattern. Although the results of this part of the study are not completely consistent with some previous reports, for example, some studies have reported a greater therapeutic effect of RPE cells induced from iPSCs (Li et al., 2022), RPE cells induced from ESCs (Sharma and Jaganathan, 2021), or RPE cells induced from MSCs after cell transplantation (Duan et al., 2017). In the present study, the improvement in the protein expression intensity index by the RPE layer was more limited in both model groups, despite the fact that significant improvement was observed in the process of the photoreceptor layer and the outer nuclear layer of the retina. Qualitative observations of treatment samples from both models, for which statistical analysis was not performed, also confirm these results **(Figure 15**). Parts of the retina that appeared to have a normal structure have been incompletely repaired in parts of the RPE layer, and in some samples, accumulation of pigmented substances could be seen in different layers of the retina.

In addition, a study reported that MSC-derived RPE transplanted cells are likely to undergo epithelial-to-mesenchymal transition (EMT), subsequently reducing the therapeutic effect of transplanted cells; if MSC-derived RPE cells exhibit anti-EMT ability, the efficacy of MSC-based therapies will be greatly improved (Zhu et al., 2022). Another study reported that the phagocytosis ability of MSC-derived RPE cells needs to be further analyzed and characterized before conclusions can be drawn regarding the differentiation of MSCs into functional RPE (Adak et al., 2021). In another study, treatment with iPSCs-RPE was more effective in delaying the loss of the photoreceptor layer in an animal model of progressive retinal degeneration compared to MSCs and neural stem cells (Li et al., 2022). Overall, this discrepancy may be due to differences in the type of stem cells, the method and site of injection, the amount of cell dose, differences in the severity and nature of the animal model injury, and differences in the duration of follow-up (Sharma and Jaganathan, 2021).

Although the results of this study provide valuable evidence about the efficacy of graft stem cells in rat AMD models, there are several limitations that should be considered in interpreting the findings. The small size in each group needs to be replicated in larger studies. In this study, only

alterations in retinal tissue structure were investigated; further work is needed to evaluate the results of retinal functional tests such as electroretinography (ERG) or optokinetic response (OKR) to determine whether the observed structural improvements translate into functional visual benefits. Although the histological results showed improvement, a comprehensive examination of molecular pathways or more precise biomarkers was not performed. This limits our ability to determine the precise mechanisms of stem cell action. The use of biocarriers, growth factors, or cell-engineering techniques can help improve cell survival and function. The failure to use these approaches in this study may have reduced the magnitude of the effect compared to some comparative studies. Ultimately, the findings of this study are another step toward understanding the potential clinical applications of stem cells, but they clearly demonstrate that further efforts are needed to improve the efficacy, safety, and predictability of the treatment to achieve sustainable and generalizable results in humans.

5. Conclusion

The findings showed that combined cell therapy in the early phase demonstrated superior structural preservation of the photoreceptor layer in the rat model, which suggests early intervention in cellular treatments of AMD. Overall, the findings of this study show that the applied therapeutic interventions had a significant and sustainable effect on the indices studied, and this effect varied depending on the type of AMD phase and treatment group; this indicates the effectiveness of the treatments and the importance of considering the phase of the disease in response to treatment. However, the limitations, as well as, the lack of retinal functional tests should be considered when interpreting the findings of this study.

Reference

1. ABOUTALEB KADKHODAEIAN, H., TIRAIHI, T., AHMADIEH, H., ZIAEI, H., DAFTARIAN, N. & TAHERI, T. 2019. Generation of retinal pigmented epithelium-like cells from pigmented spheres differentiated from bone marrow stromal cell-derived neurospheres. *Tissue engineering and regenerative medicine,* 16**,** 253-263.

2. ABOUTALEBKADKHODAEIAN, H., SAMENI, H. & SHAHBAZI, A. 2021. Neurosphere-free transdifferentiation of rat bone marrow stromal stem cells into retinal cells and retinal pigment epithelium. *Basic and Clinical Neuroscience,* 12**,** 617.

3. ADAK, S., MAGDALENE, D., DESHMUKH, S., DAS, D. & JAGANATHAN, B. G. 2021. A review on mesenchymal stem cells for treatment of retinal diseases. *Stem cell reviews and reports,* 17**,** 1154-1173.

4. BARZELAY, A., WEISTHAL ALGOR, S., NIZTAN, A ,.KATZ, S., BENHAMOU, M., NAKDIMON, I., AZMON, N., GOZLAN, S., MEZAD-KOURSH, D. & NEUDORFER, M. 2018. Adipose-Derived Mesenchymal Stem Cells Migrate and Rescue RPE in the Setting of Oxidative Stress. *Stem Cells International,* 2018**,** 9682856.

5. BLASIAK, J., PIECHOTA, M., PAWLOWSKA, E., SZATKOWSKA, M., SIKORA, E. & KAARNIRANTA, K. 2017. Cellular senescence in age-related macular degeneration: can autophagy and DNA damage response play a role? *Oxidative Medicine and Cellular Longevity,* 2017**,** 5293258.

6. CHEN, F., LIU, X., CHEN, Y., LIU, J. Y., LU, H., WANG, W., LU, X., DEAN, K. C., GAO, L. & KAPLAN, H. J. 2020. Sphere-induced reprogramming of RPE cells into dual-potential RPE stem-like cells. *EBioMedicine,* 52.

7. CHICHAGOVA, V., HALLAM, D., COLLIN, J., ZERTI, D., DORGAU, B., FELEMBAN, M., LAKO, M. & STEEL, D. H. 2018. Cellular regeneration strategies for macular degeneration: past, present and future. *Eye,* 32**,** 946-971.

8. CHOW, L. L. & MEAD, B. 2023. Extracellular vesicles as a potential therapeutic for age-related macular degeneration. *Neural Regeneration Research,* 18**,** 1876-1880.

9. DENG, Y., QIAO, L., DU, M., QU, C., WAN, L., LI, J. & HUANG, L. 2022. Age-related macular degeneration: Epidemiology, genetics, pathophysiology, diagnosis, and targeted therapy. *Genes & diseases*.۶۲-۷۹ ,۹ ,

10. DINIZ, B., THOMAS, P., THOMAS, B., RIBEIRO, R., HU, Y., BRANT, R., AHUJA, A., ZHU, D., LIU, L. & KOSS, M. 2013. Subretinal implantation of retinal pigment epithelial cells derived from human embryonic stem cells: improved survival when implanted as a monolayer. *Investigative ophthalmology & visual science,* 54**,** 5087-5096.

11. DUAN, P., ZENG, Y., LIU, Y., WANG, Y., XU, H. & YIN, Z. 2017. Comparison of protective effects of hESCs-derived and hBMSCs-derived RPE cells on sodium iodate-injuried rat retina. *Int. J. Clin. Exp. Pathol,* 10**,** 5274-5284.

12. ENZMANN, V., ROW, B. W., YAMAUCHI, Y., KHEIRANDISH, L., GOZAL, D., KAPLAN, H. J. & MCCALL, M. A. 2006. Behavioral and anatomical abnormalities in a sodium iodate-induced model of retinal pigment epithelium degeneration. *Experimental eye research,* 82**,** 441-448.

13. FINOCCHIO, L., ZEPPIERI, M., GABAI, A., SPADEA, L. & SALATI, C. 2023. Recent advances of adipose-tissue-derived mesenchymal stem cell-based therapy for retinal diseases. *Journal of clinical medicine,* 12.٧٠١٥ ,

14. GEATHERS, J. S., GRILLO, S. L., KARAKOLEVA, E., CAMPBELL, G. P., DU, Y., CHEN, H., BARBER, A. J., ZHAO, Y. & SUNDSTROM, J. M. 2024. Sodium Iodate: Rapid and Clinically Relevant Model of AMD. *Frontiers in Bioscience-Landmark,* 29**,** 380.

15. HANUS, J., ANDERSON, C., SARRAF, D., MA, J. & WANG, S. 2016. Retinal pigment epithelial cell necroptosis in response to sodium iodate. *Cell death discovery,* 2**,** 1-9.

16. HOLAN, V., PALACKA, K. & HERMANKOVA, B. 2021. Mesenchymal stem cell-based therapy for retinal degenerative diseases: experimental models and clinical trials. *Cells,* 10**,** 588.

17. HU, C., LA, H., WEI, X., ZHOU, Y., OU, Q., CHEN, Z., ZHU, X., XU, J.-Y., JIN, C. & GAO, F. 2020. Transplantation site affects the outcomes of adipose-derived stem cell-based therapy for retinal degeneration. *Stem cells international,* 2020**,** 9625798.

18. IRIGOYEN, C., AMENABAR ALONSO, A., SANCHEZ-MOLINA, J., RODRÍGUEZ-HIDALGO, M., LARA-LÓPEZ, A. & RUIZ-EDERRA, J. 2022. Subretinal injection techniques for retinal disease: a review. *Journal of clinical medicine,* 11**,** 4717.

19. KADKHODAEIAN, H. A., SALATI, A. & LASHAY, A. 2019. High efficient differentiation of human adipose-derived stem cells into retinal pigment epithelium-like cells in medium containing small molecules inducers with a simple method .*Tissue and Cell,* 56**,** 52-59.

20. KADKHODAEIAN, H. A., TIRAIHI, T., AHMADIEH, H., ARDAKANI, H. Z., DAFTARIAN, N. & TAHERI, T. 2018. Survival and migration of adipose-derived stem cells transplanted in the injured retina. *Experimental and Clinical Transplantation,* 16**,** 204-11.

21. KADKHODAEIAN, H. A., TIRAIHI, T., DAFTARIAN, N., AHMADIEH, H., ZIAEI, H. & TAHERI, T. 2016. Histological and electrophysiological changes in the retinal pigment epithelium after injection of sodium iodate in the orbital venus plexus of pigmented rats. *Journal of Ophthalmic & Vision Research,* 11**,** 70.

22. LI, L., YU, Y., LIN, S. & HU, J. 2022. Changes in best-corrected visual acuity in patients with dry age-related macular degeneration after stem cell transplantation: systematic review and meta-analysis. *Stem Cell Research & Therapy,* 13**,** 237.

23. LIN, Y., REN, X., CHEN, Y. & CHEN, D. 2021. Interaction between mesenchymal stem cells and retinal degenerative microenvironment. *Frontiers in Neuroscience,* 14**,** 617377.

24. MORIGUCHI, M., NAKAMURA, S., INOUE ,Y., NISHINAKA, A., NAKAMURA, M., SHIMAZAWA, M. & HARA, H. 2018. Irreversible photoreceptors and RPE cells damage by intravenous sodium iodate in mice is related to macrophage accumulation. *Investigative ophthalmology & visual science,* 59**,** 3476-3487.

25. PARIKH, S., LE, A., DAVENPORT, J., GORIN, M. B., NUSINOWITZ, S. & MATYNIA, A. 2016. An alternative and validated injection method for accessing the subretinal space via a transcleral posterior approach. *Journal of visualized experiments: JoVE***,** 54808.

26. PAWLOWSKA ,E., SZCZEPANSKA, J., KOSKELA, A., KAARNIRANTA, K. & BLASIAK, J. 2019. Dietary polyphenols in age-related macular degeneration: protection against oxidative stress and beyond. *Oxidative medicine and cellular longevity,* 2019**,** 9682318.

27. PINELLI, R., BIAGIONI, F., LIMANAQI, F., BERTELLI, M., SCAFFIDI, E., POLZELLA, M., BUSCETI, C. L. & FORNAI, F. 2020. A re-appraisal of pathogenic mechanisms bridging wet and dry age-related macular degeneration leads to reconsider a role for phytochemicals. *International Journal of Molecular Sciences,* 21**,** 5563.

28. QU, L., GAO, L., XU, H., DUAN, P., ZENG, Y., LIU, Y. & YIN, Z. Q. 2017. Combined transplantation of human mesenchymal stem cells and human retinal progenitor cells into the subretinal space of RCS rats. *Scientific reports,* 7**,** 199.

29. SHARMA, A. & JAGANATHAN, B. G. 2021. Stem cell therapy for retinal degeneration: the evidence to date. *Biologics: Targets and Therapy***,** 299-306.

30. SINGH, M. S. & MACLAREN, R. E. 2018. Stem cell treatment for age-related macular degeneration: the challenges. *Investigative ophthalmology & visual science,* 59**,** AMD78-AMD82.

31. THOMAS, C. N., SIM, D. A., LEE, W. H., ALFAHAD, N., DICK, A. D., DENNISTON, A. K. & HILL, L. J. 2022. Emerging therapies and their delivery for treating age-related macular degeneration. *British journal of pharmacology,* 179**,** 1908-1937.

32. TRINCAO-MARQUES, J., AYTON, L. N., HICKEY, D. G., MARQUES-NEVES, C., GUYMER, R. H., EDWARDS, T. L. & SOUSA, D. C. 2024. Gene and cell therapy for age-related macular degeneration: A review. *Survey of Ophthalmology,* 69**,** 665-676.

33. WANG, Z., GAO, F., ZHANG, M., ZHENG, Y., ZHANG, F., XU, L., CAO, L. & HE, W. 2020. Intravitreal injection of human retinal progenitor cells for treatment of retinal degeneration. *Medical Science Monitor: International Medical Journal of Experimental and Clinical Research,* 26**,** e921184-1.

34. YANG, E., LIU, N., TANG, Y., HU, Y., ZHANG, P., PAN, C., DONG, S., ZHANG, Y. & TANG, Z. 2015. Generation of neurospheres from human adipose-derived stem cells. *BioMed research international*.٧٤٣٧١٤ ,٢٠١٥ ,

35. YANG, Y.-P., HSIAO, Y.-J., CHANG, K.-J., FOUSTINE, S., KO, Y.-L., TSAI, Y.-C., TAI, H.-Y., KO, Y.-C., CHIOU, S.-H. & LIN, T.-C. 2022. Pluripotent stem cells in clinical cell transplantation: focusing on induced pluripotent stem cell-derived RPE cell therapy in age-related macular degeneration. *International journal of molecular sciences,* 23**,** 13794.

36. YARDENI, T., ECKHAUS, M., MORRIS, H. D., HUIZING, M. & HOOGSTRATEN-MILLER, S. 2011. Retro-orbital injections in mice. *Lab animal,* 40**,** 155-160.

37. YOUNG, B. M., JONES, K., MASSENGILL, M. T., WALSH, E., LI, H., LEWIN, A. S. & ILDEFONSO, C. J. 2019. Expression of a CARD slows the retinal degeneration of a geographic atrophy mouse model. *Molecular Therapy Methods & Clinical Development,* 14**,** 113-125.

38. ZAQOUT, S., BECKER, L.-L. & KAINDL, A. M. 2020. Immunofluorescence staining of paraffin sections step by step. *Frontiers in neuroanatomy,* 14**,** 582218.

39. ZHAI, W., GAO, L., QU, L., LI, Y., ZENG, Y., LI, Q., XU, H. & YIN, Z. Q. 2020. Combined transplantation of olfactory ensheathing cells with rat neural stem cells enhanced the therapeutic effect in the retina of RCS rats. *Frontiers in cellular neuroscience,* 14**,** 52.

40. ZHANG, Y., ZHANG, D., WEI, W., SHEN, B., WANG, Y., ZHANG, Y., ZHANG, Y., JI, J., SUN, H. & LUO, M .٢٠١٧ .Effects of RPE-conditioned medium on the differentiation of

hADSCs into RPE cells, and their proliferation and migration. *Experimental and Therapeutic Medicine,* 14**,** 3699-3707.

41. ZHANG, Z.-Y., BAO, X.-L., CONG, Y.-Y., FAN, B. & LI, G.-Y. 2020. Autophagy in age-related macular degeneration: a regulatory mechanism of oxidative stress. *Oxidative medicine and cellular longevity,* 2020**,** 2896036.

42. ZHU, X., CHEN, Z., WANG, L., OU, Q., FENG, Z., XIAO, H., SHEN, Q., LI, Y., JIN, C. & XU, J.-Y. 2022. Direct conversion of human umbilical cord mesenchymal stem cells into retinal pigment epithelial cells for treatment of retinal degeneration. *Cell death & disease,* 13**,** 785

Figure 1: Rational and aim of the study.

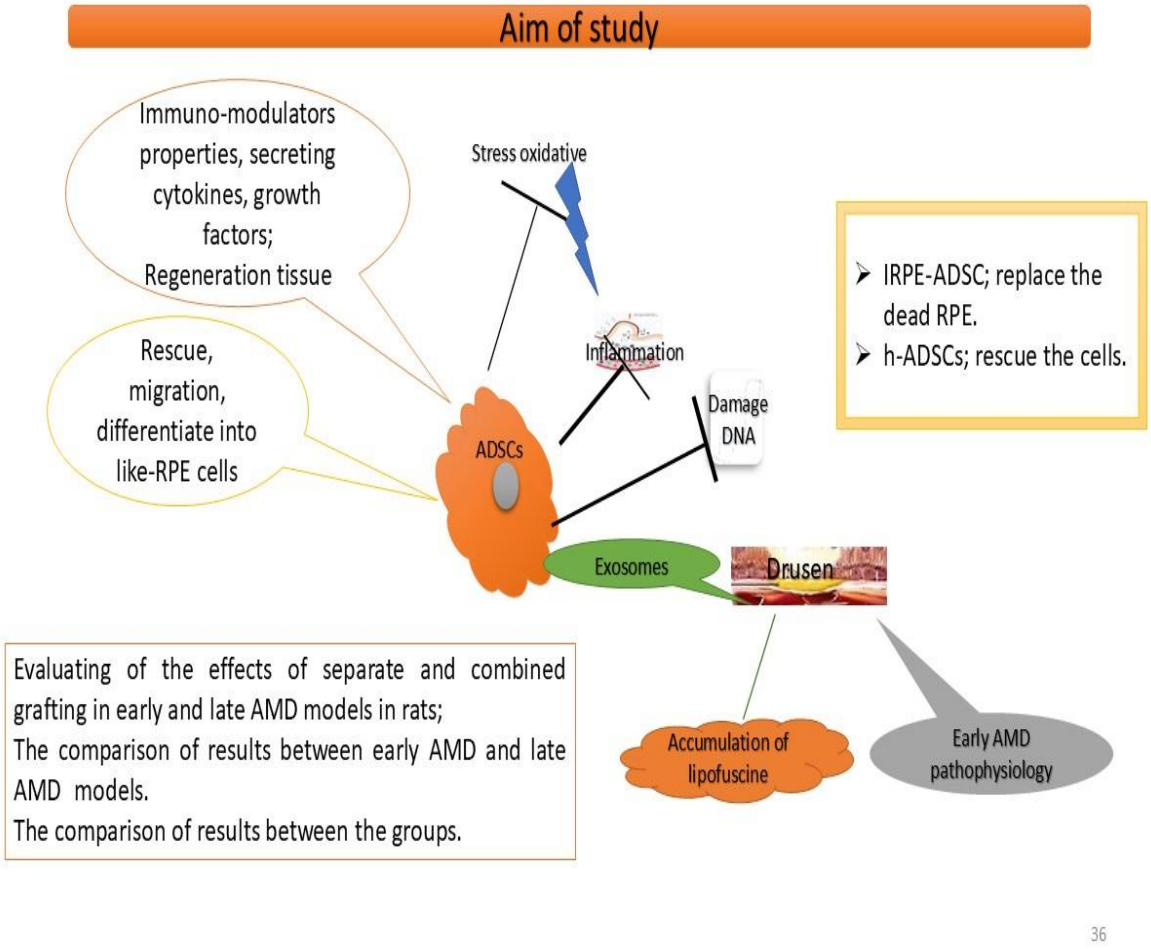

Fig. 1. Summary and schematic image of the effects of the two cells investigated in this study for treating damaged retinal pigment epithelium in an age-related macular degeneration model.

Figure 2: Study phases and design.

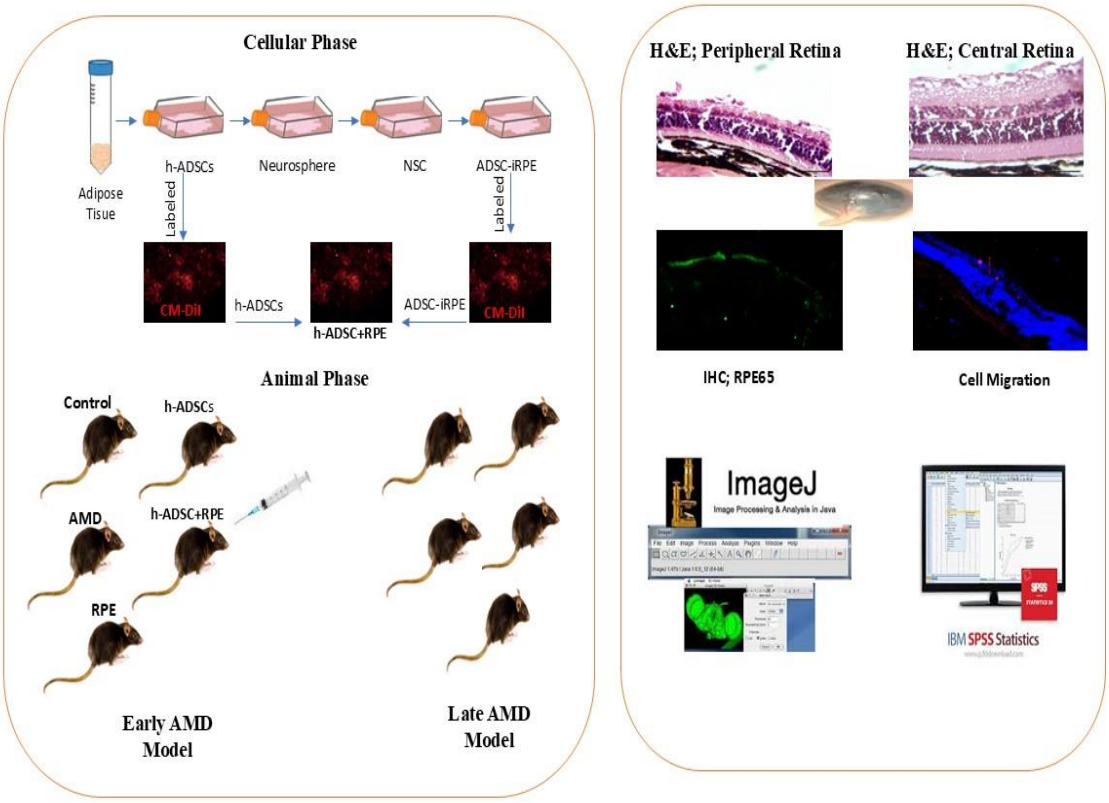

Fig. 2. Schematic representation of the study design. Cellular phase: Adipose tissue- stem cells (h-ADSCs) were isolated, cultured, and first induced into neurospheres, then neural stem cells, and finally into RPE cells. Morphological evaluations by immunocytochemistry confirmed the expression of cell-specific markers. Animal phase: Following induction of the AMD model, h-ADSC and ADSC-iRPE cells and their combination were transplanted subretinally into the rat eyes. Then, during the follow-up period, the condition of the retinal layers, cell survival, and histological analysis were evaluated. This diagram summarizes the overall study design from cell preparation to the final assessment in the animal model.

Table 1: Study Samples

Early AMD Model Group	Late AMD Model Group	Retrobulbar injection	Subretinal Transplantation Time (Early AMD)	Subretinal Transplantation Time (Late AMD)	Transplanted cell type
E.Control	L.Control	PBS		-	-
E.AMD	L.AMD	Sodium Iodide	1 Days after model creation	15 Days after model creation	PBS
E.AMD+ h-ADSC	L.AMD+ h-ADSC	Sodium Iodide	1 Day after model creation	15 Days after model creation	h-ADSC
E.AMD+ RPE	L.AMD+ RPE	Sodium Iodide	1 Day after model creation	15 Days after model creation	RPE
E.AMD+h-ADSC+RPE	L.AMD+h-ADSC+RPE	Sodium Iodide	1 Day after model creation	15 Days after model creation	h-ADSC+RPE

The study samples (60 adult male pigmented rats) were randomly divided into 10 equal groups, each group containing 6 rats; 5 groups were selected for the early AMD model and 5 groups for the late AMD model.

E, Early; L, Late; h, Human

Figure 3: Human adipose tissue-derived stem cells (h-ADSC).

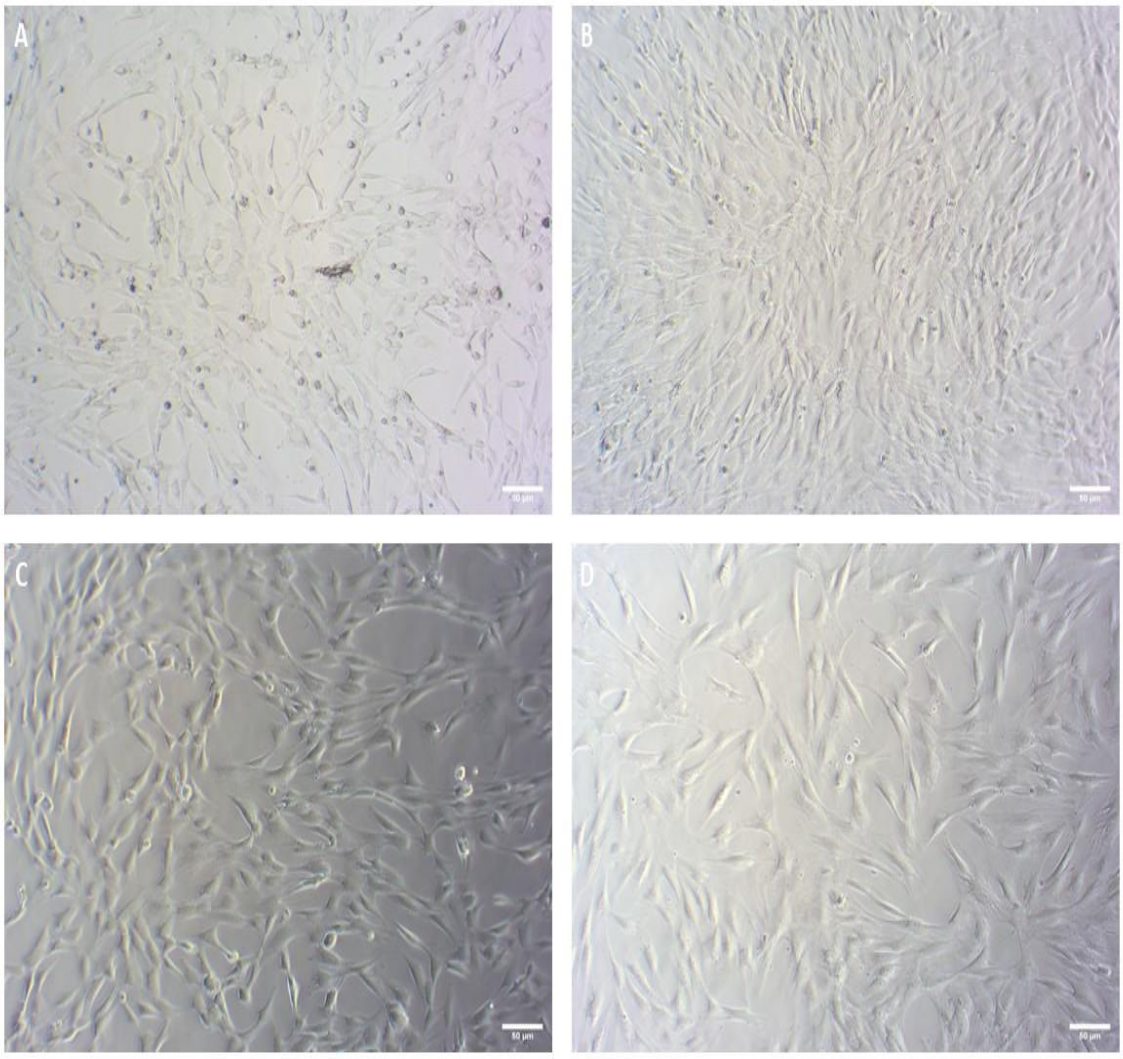

Fig. 3. Light microscope view of human adipose tissue-derived stem cells at different cell passages. **A**: Image of passage 0 ADSC cells with 85% confluency, **B**: Passage 1 ADSC cells with 90% confluency, **C**: Passage 2 ADSC cells with 85% confluency, and **D**: Passage 3 ADSC cells with 80% confluency. The purity of ADSCs increases as they are passaged more frequently (Scale bar: 50µm).

Figure 4: Immunocytochemical stained ADSCs.

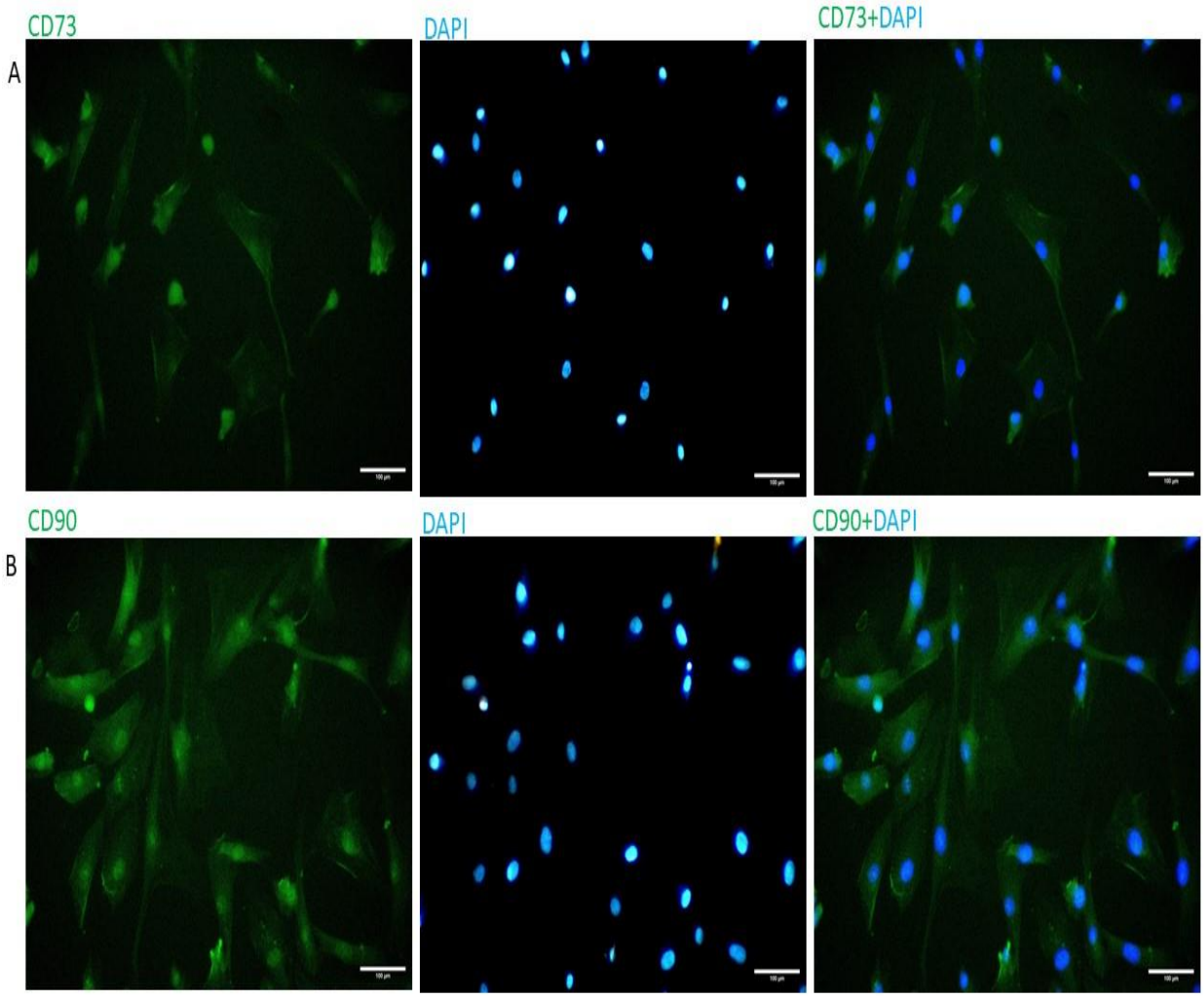

Fig. 4. Images taken with an Olympus inverted fluorescent microscope show immunocytochemical staining of ADSCs. **A:** Positive reaction of ADSCs with the CD73 marker, **B:** Positive reaction of ADSCs with the CD90 marker. Green indicates CD73 and CD90, blue indicates DAPI, and blue and green show the overlap of the first and second images (Scale bar: 100 µm).

Figure 5: Stages of neurosphere formation from adipose-derived stem cells (ADSCs).

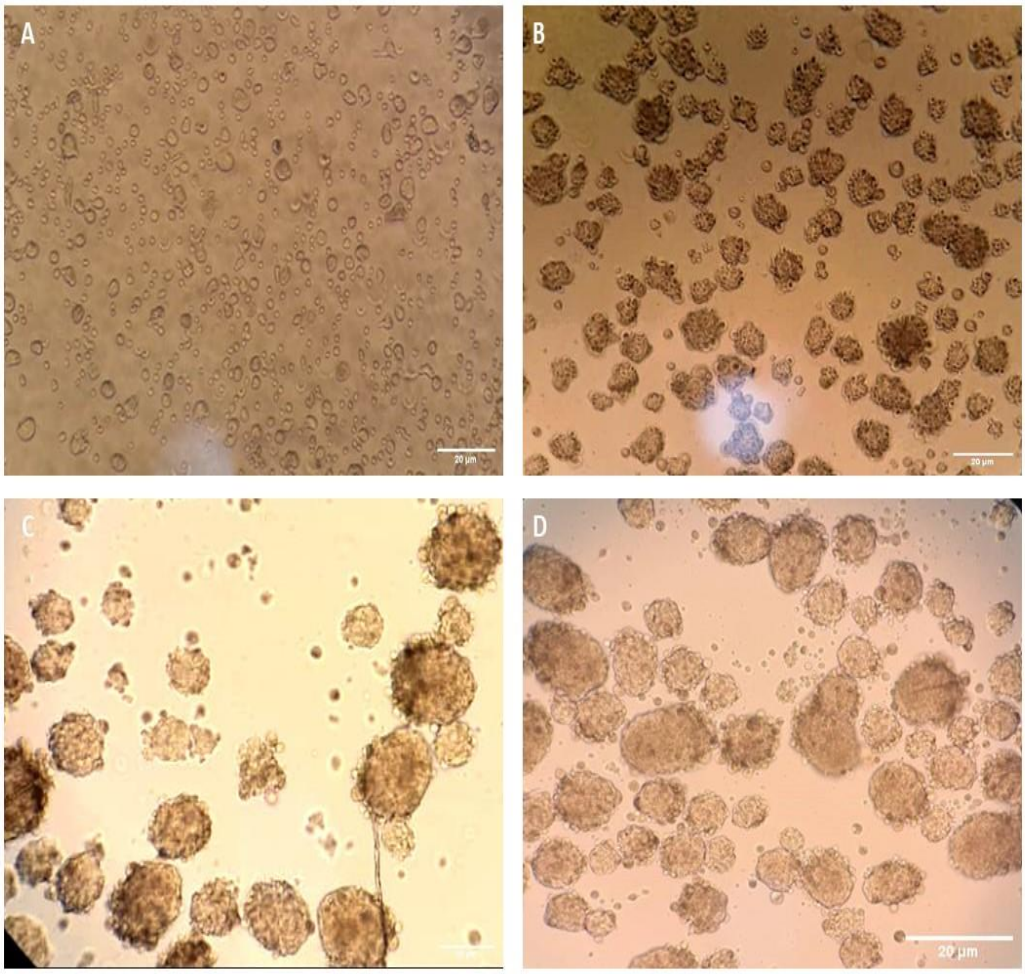

Fig. 5. Images of the stages of growth and formation of neurospheres from adipose-derived stem cells (ADSCs) with an inverted fluorescent microscope. **A**: The first day of culture of fourth-passage h-ADSCs in neurosphere medium. **B**: On the third day of culture, the cells are colonizing. **C**: On the ninth day of culture, the cells gradually change shape and become spherical. **D**: On the 12th day of cell culture, the final stages of growth are characterized by a round shape with spikes attached to their periphery (Scale bar: 20 µm).

Figure 6: Formation of neural stem cells differentiated from ADSC-derived neuropheres.

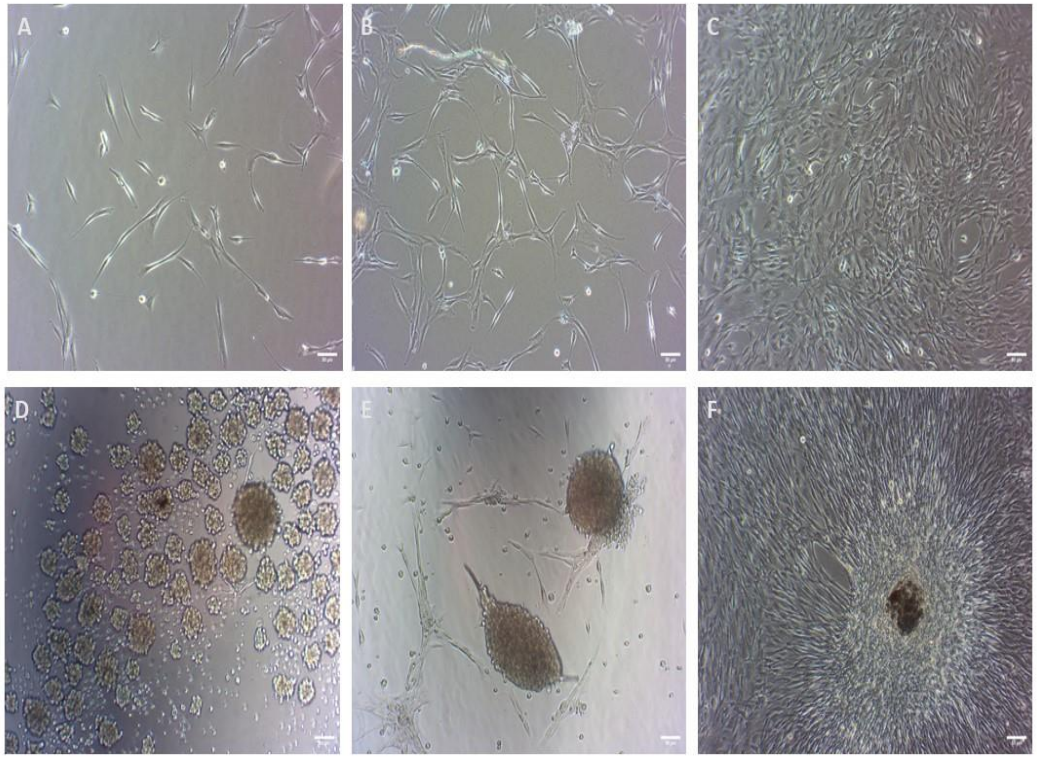

Fig. 6. Images of the stages of growth and formation of neural stem cells differentiated from ADSC-derived neuropheres with an inverted microscope. **A**–**C:** the proliferation and growth of separated cells that have maintained their fibroblastic shape and proliferated; **D**- **F:** undissociated neurospheres in the neural stem cell medium, where growth begins from the center and has proliferated (Scale bar: 50 µm).

Figure 7: Stages of neural stem cell differentiation into RPE.

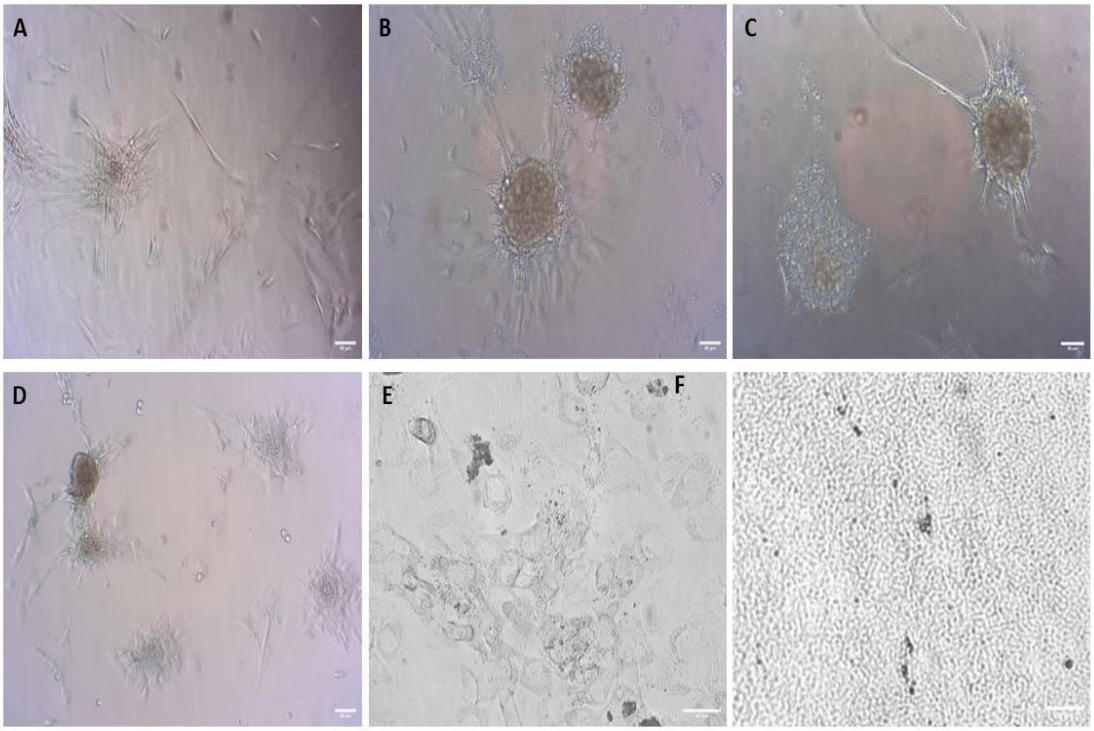

Fig. 7. Images of the stages of neural stem cell differentiation into RPE using an inverted microscope. Figure **A** shows the second day of differentiation of neural stem cells derived from adipose tissue stem cells in the RPE differentiation medium; the cells are both fibroblast-like and spherical, and the cells are growing from the edges of the spherical cells. Figure **B**: On the 7th day of differentiation culture, the cells continue to grow and proliferate and are changing shape. **C**: On the 14th day of differentiation culture, the cells are becoming cuboidal and changing color. **D**: On the 17th day, the cuboidal cells have proliferated from the sides and joined together. **E**: Day 22, spherical cells are disappearing and the bottom of the plate is almost filled with cuboidal cells and fibroblasts. **F**: Areas of the bottom of the plate showing a single layer of cuboidal and pigmented cells. (**A- D)**: Scale bar is 50 µm, (**E and F)**: scale bar is 20 µm).

Figure 8: RPE cells differentiated from ADSC-derived neural stem cells (NSCs).

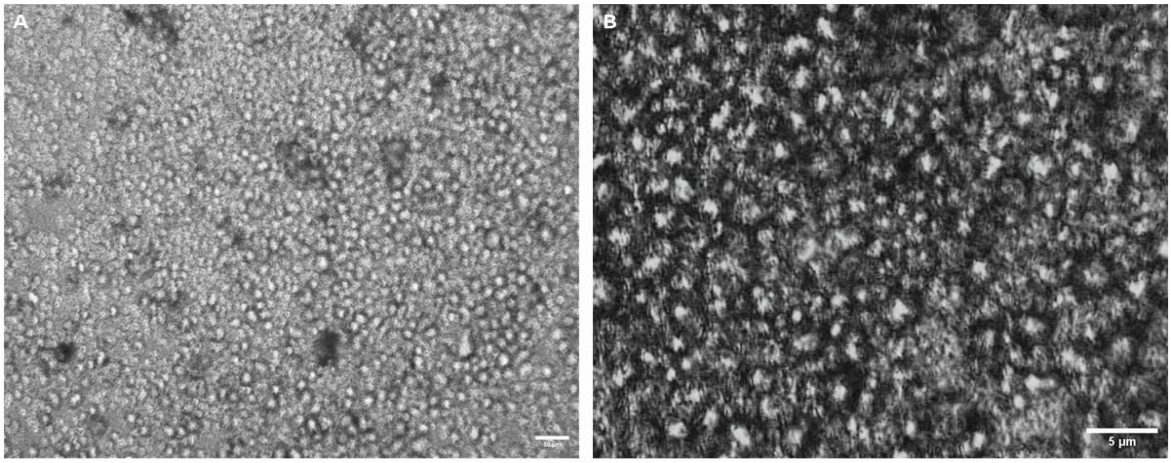

Fig. 8. RPE cells differentiated from ADSC-derived NSCs before the second cell passage used in the study (with different magnifications). (**A**: Scale bar: 50 µm, **B**: Scale bar: 5 µm).

Figure 9: Staining of differentiated neural stem cell (NSC)-derived RPE cells with RPE65.

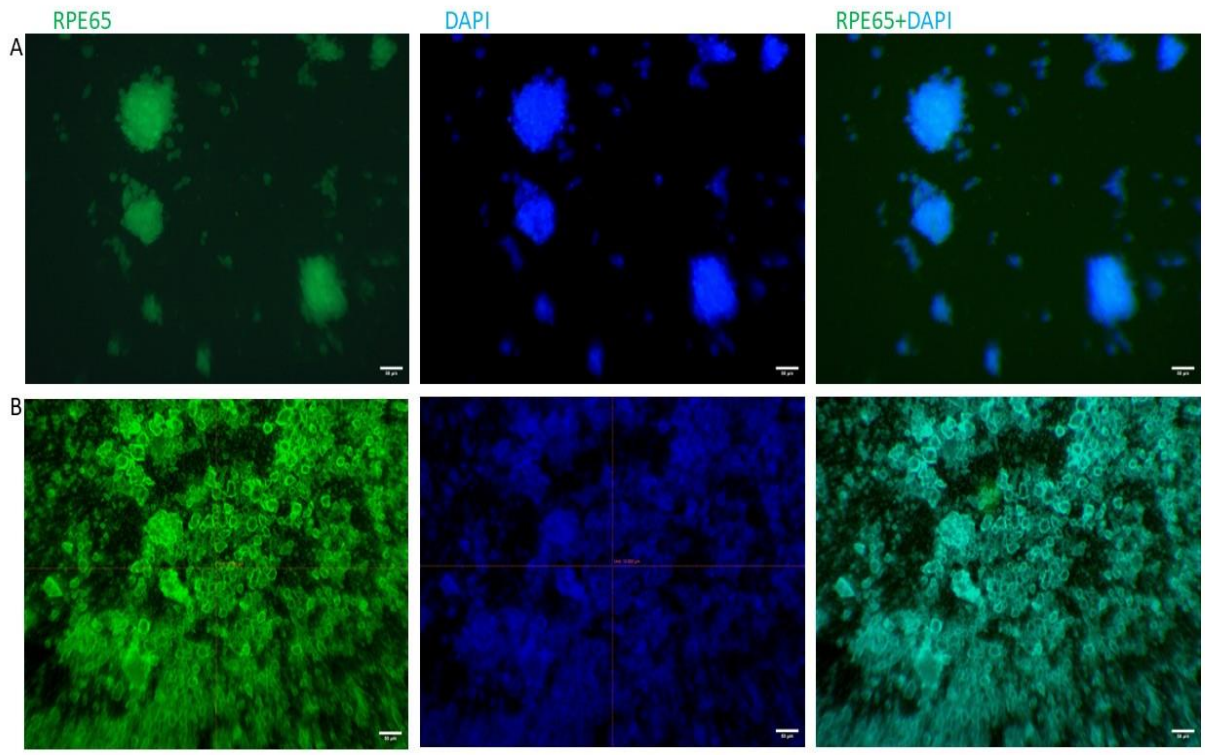

Fig. 9. Images of differentiated NSC-derived RPE cells with their positive reaction to the RPE65 marker by inverted fluorescence microscopy. **A**: the cells stained with positive reaction to the RPE65 antibody before the first cell passage. **B**: the cells stained with a positive reaction to the RPE65 antibody before the second cell passage. Apparently, the pattern and extent of staining (indicating the level of RPE65 protein expression by RPE cells) is different between the two cell passages. Green color indicates the RPE65 antibody, blue color indicates DAPI, and blue and green indicate the overlap of the first and second images (Scale bar: 50 µm).

Figure 10: Histological images of the retina in different studied groups (peripheral and central areas of the retina).

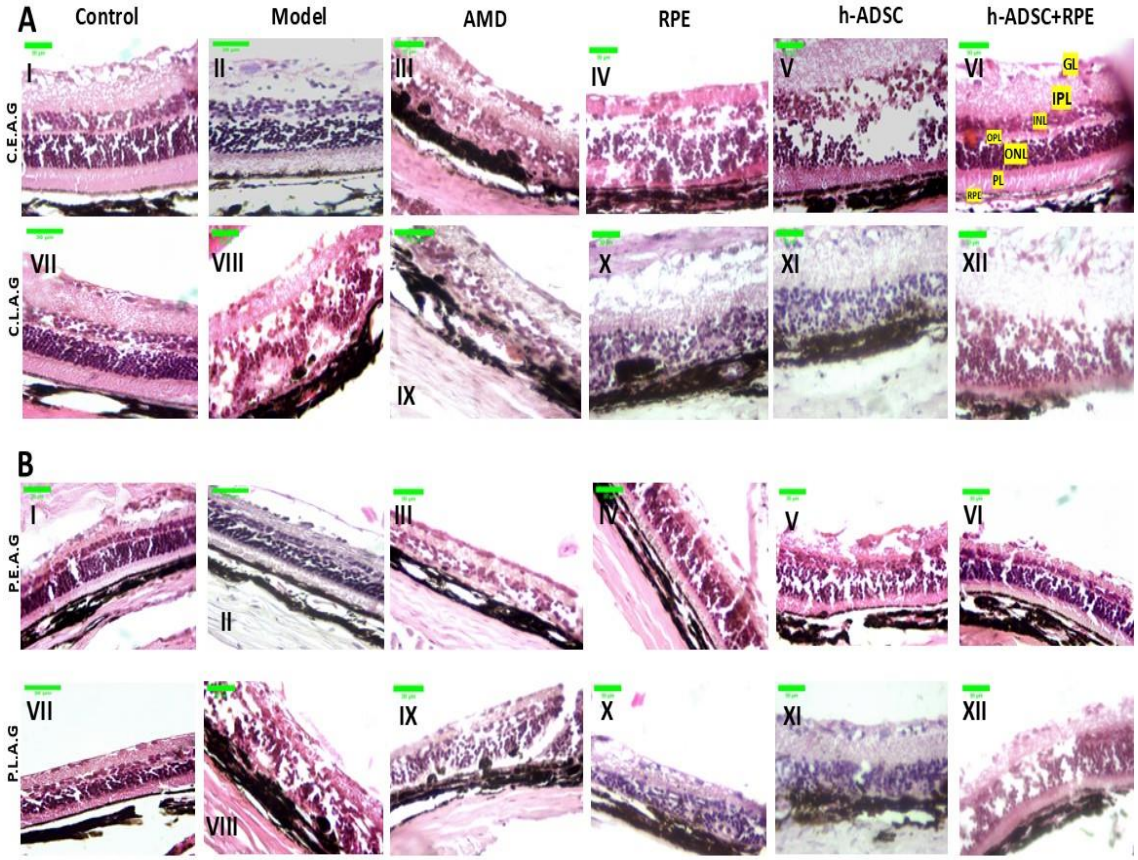

Fig. 10. Microscopic images of the retina of rats in different studied groups in the peripheral and central areas, with H&E staining. In the untreated group (AMD), a decrease in the thickness of the retinal layers and a disruption of the cellular structure are observed compared to the control group. In the groups receiving treatment (RPE, h-ADSC, h-ADSC+RPE), a relative preservation of the layered organization and an increase in the thickness of the retina are observed compared to the untreated group. **A** (I-VI): representative images of the central part of the retina of the five groups (I, III, IV, V, VI) in the early AMD model, and 24 hours after sodium iodide injection at a dose of 25 mg/kg and before transplantation (II); **A** (VII-XII): representative images of the central part of the retina in the late AMD model. **B** (I-VI and VII-XII): representative images of the peripheral part of the retina. C.E.A.G (central early AMD groups), C.L.A.G (central late AMD groups), P.E.A.G (peripheral early AMD groups), P.L.A.G (peripheral late AMD groups) (Scale bar: 30 µm).

Table 2 Early Age-Related Macular Degeneration (AMD) Model

Variable (Area)	E.Control (µm)	E.AMD (µm)	E.RPE (µm)	E.ADSC (µm)	E.ADSC+RPE (µm)
PLT (P)	9.55±1.69	2.05±0.68	8.87±0.89	8.71±2.70	9.47±1.99
PLT (C)	18.72±4.09	1.99±0.63	10.06±2.30	10.15±3.02	16.86±3.38
PLT (T)	14.14±1.55	2.02±0.65	9.46±0.86	9.43±2.63	13.16±2.54
ONLN (P)	3.45±0.12	0.90±0.57	2.90±0.91	2.83±0.43	3.32±0.21
ONLN (C)	4.68±0.38	0.87±0.58	2.91±0.41	2.85±0.33	4.48±0.81
ONLN (T)	4.06±0.25	0.88±0.57	2.90±0.23	2.84±0.31	3.90±0.43
RPE65 Intensity	3.33±0.99	0.63±0.34	1.30±0.57	1.11±0.40	2.20±0.70

Mean±standard deviation of photoreceptor layer thickness (PLT) and the number of outer retinal nuclear layer rows (ONLN) in peripheral (P), central (C) and total areas (T: average of peripheral and central) and the intensity of RPE65 protein expression by the retinal pigment epithelium layer in the early AMD groups. Data are reported as mean±standard deviation (4 slides per retinal area, and 4 rats per group).

Table 3. Late Age-Related Macular Degeneration (AMD) Model

Variable (Area)	L.Control (µm)	L.AMD (µm)	L.RPE (µm)	L.ADSC (µm)	L.ADSC+RPE (µm)
PLT (P)	10.79±0.34	1.82±0.43	3.92±0.97	3.91±0.67	5.29±1.80
PLT (C)	18.82±1.64	1.70±0.45	4.57±1.71	6.01±1.58	9.06±1.88
PLT (T)	14.81±0.76	1.76±0.21	4.25±1.21	4.96±0.92	7.17±1.75
ONLN (P)	3.36±0.22	0.90±0.71	1.11±0.51	1.52±0.72	1.62±0.31
ONLN (C)	5.02±0.28	0.83±0.72	1.75±0.82	1.62±0.58	2.50±0.91
ONLN (T)	4.19±0.21	0.86±0.33	1.43±0.66	1.57±0.50	2.06±0.11
RPE65 Intensity	3.39±1.03	0.66±0.17	1.22±0.49	0.97±0.43	1.51±0.72

Mean±standard deviation of photoreceptor layer thickness (PLT) and the number of outer retinal nuclear layer rows (ONLN) in peripheral (P)**,** central (C) and total areas (T: average of peripheral and central) and the intensity of RPE65 protein expression by the retinal pigment epithelium layer in the late AMD groups. Data are reported as mean±standard deviation (4 slides per retinal area, and 4 rats per group).

Figure 11: Histological diagram in different studied groups (peripheral, central, and the whole retina).

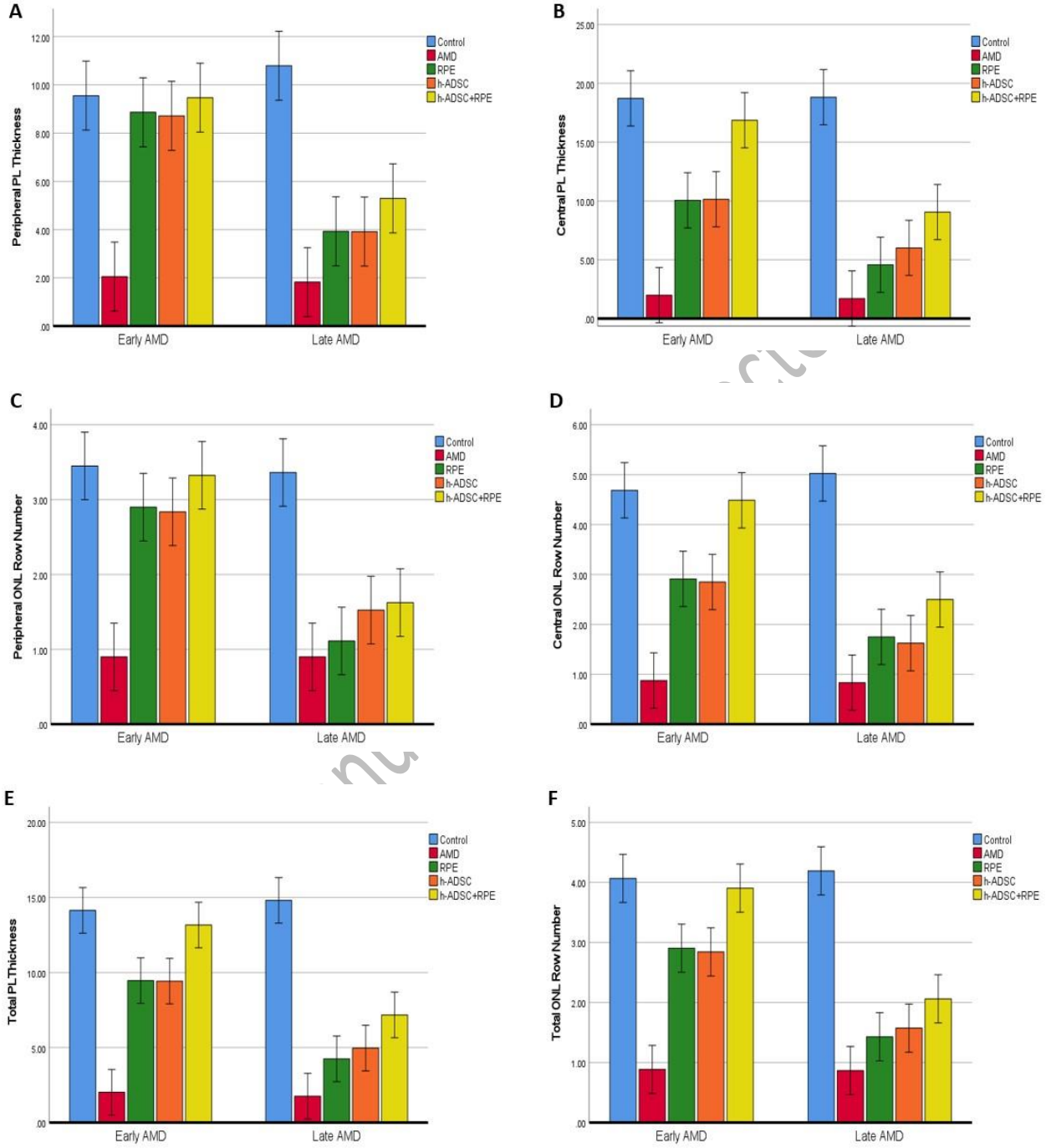

Illustration of the average photoreceptor layer thickness and the number of outer nuclear layer rows in the peripheral and central retina, and the total (average of the peripheral and central areas of the retina), in two early and late AMD models and five different treatment groups. The results reveal that the means of all variables are different between the early AMD and late AMD model groups; the highest means are observed in the control groups and the lowest in the AMD groups ($P < 0.001$). A and C show the chart of photoreceptor layer thickness and the number of outer nuclear layer rows in the peripheral retina, B and D represent these variables in the central retina, respectively, and E and F indicate the chart of the average photoreceptor layer thickness and the number of outer nuclear layer rows in the peripheral and central retina, respectively. For all these variables, the main effects of the model and the group, as well as the interaction effect of phase × treatment, were significant ($p \leq 0.001$). In the early AMD model, there was a different pattern in the early model's treatment responses to PLT and ONLN in the peripheral and central parts of the retina. In the peripheral part, there was a significant difference between the AMD group and the other groups ($p < 0.001$); in the central part, except for this case ($p < 0.01$), there was a significant difference between the control group and the two E.AMD + RPE and E.AMD + h-ADSC groups ($p < 0.01$). For the mean PLT and ONLN of the whole retina, the statistical results were almost similar to those of the central part. In the late AMD model, there was a significant difference between the mean PLT (P, C) and ONLN (P, C) in the L.Control group compare to the other groups ($P \leq 0.001$).

ONL; outer nuclear layer, PL; photoreceptors layer, PLT; photoreceptor layer thickness, ONLN; outer nuclear layer rows number, PLT (P, C); photoreceptor layer thickness (peripheral, central), ONLN (P, C); outer nuclear layer rows number (peripheral, central).

Figure 12: Distribution of transplanted cells in different retinal layers.

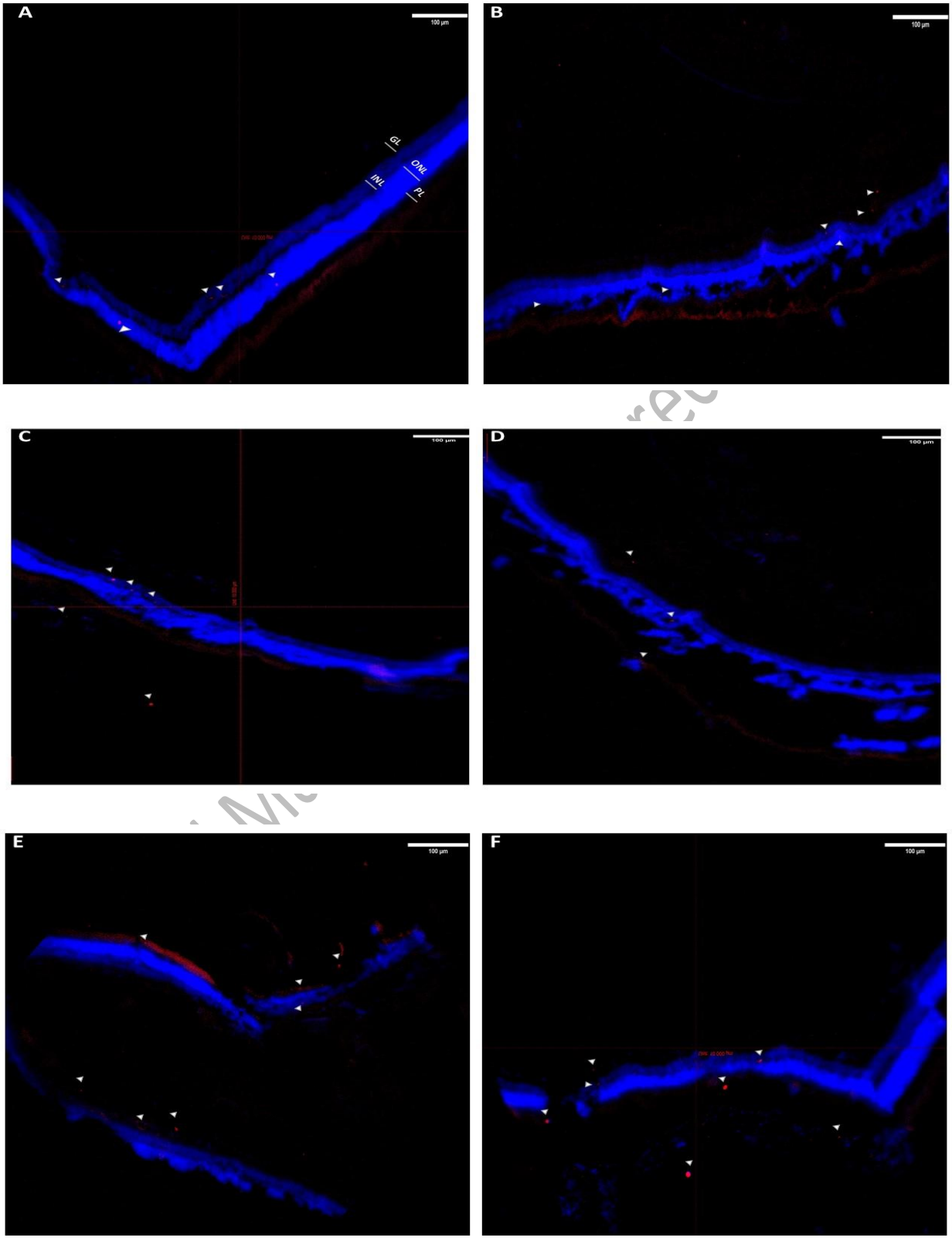

Microscopic images of the distribution of transplanted cells in different retinal layers. After transplantation, the cells settled in the damaged areas and were located in the photoreceptor and inner retinal layers, indicating their targeted migration and regenerative role. **A**: the group that received combined cells in the Early AMD model (E.AMD + h-ADSC + RPE); **B**: the group that received combined cells in the late AMD model (L.AMD+h-ADSC+RPE); **C**: the early AMD model group that received h-ADSC (E.AMD + h-ADSC); **D**: the late AMD model group that received h-ADSC (L.AMD + h-ADSC); **E**: the early AMD model group that received RPE-like cells (E.AMD + RPE); F the late AMD model group that received RPE-like cells (L.AMD + RPE). White arrows indicate cell migration to the retinal layers, and red dots represent the graft cells.

PL; photoreceptors layer, ONL; outer nuclear layer, INL; inner nuclear layer, GL; ganglion layer (Scale Bar: 100 μm).

Figure 13: Immunohistochemical alterations in the expression of RPE65 protein in different studied groups.

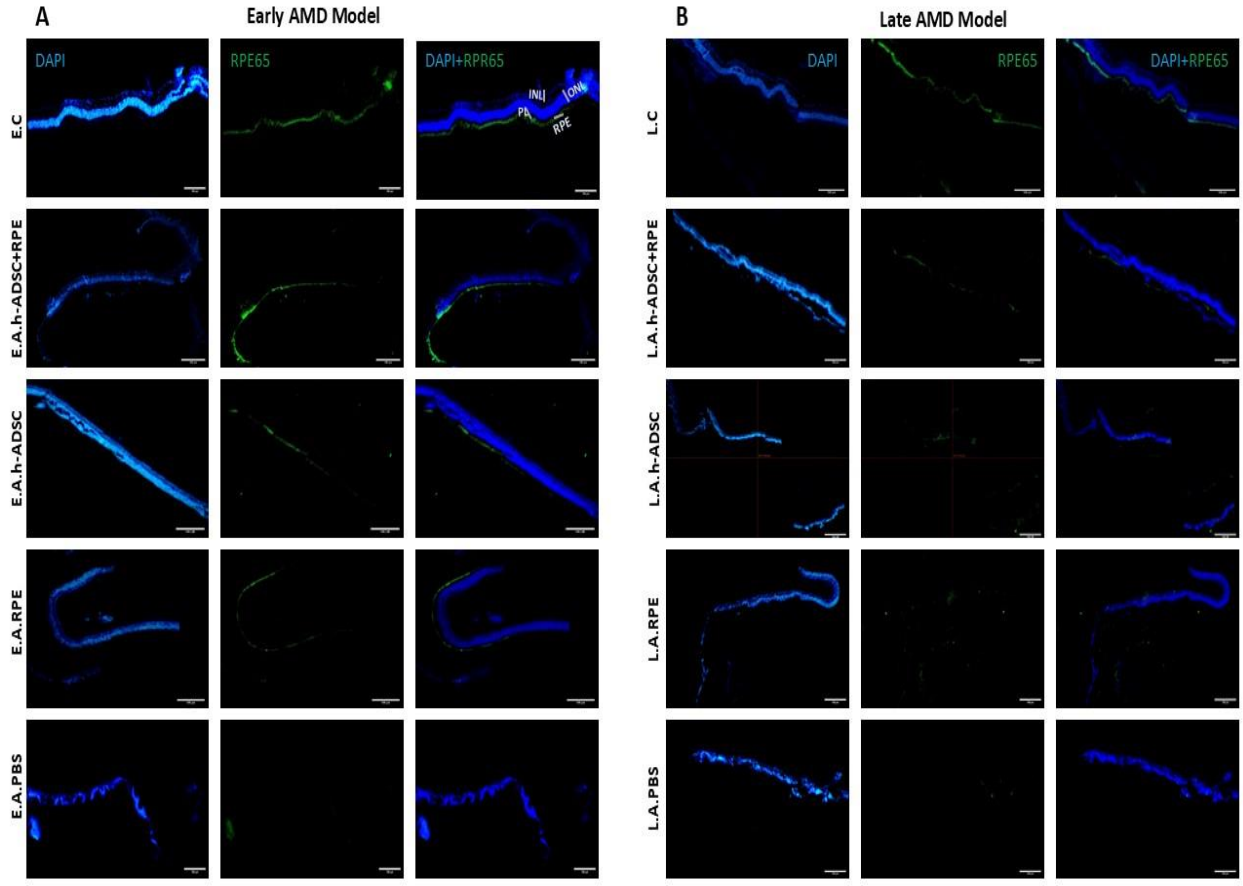

Images of immunohistochemical alterations in the expression of the RPE65 protein by the retinal pigment epithelium layer in the different studied groups using an inverted fluorescent microscope. The intensity of staining indicates the level of RPE65 protein expression. A shows stained retinas of the 5 groups in the early AMD model, and B represents the groups in the late AMD model. In the control groups (healthy rats), a uniform and regular distribution of RPE65 protein expression is observed, whereas in the AMD groups (received PBS), a significant decrease in the level of protein expression is observed. Green indicates the RPE65 antibody, blue indicates DAPI, and blue and green indicate the overlap of the first and second images.

E.C (control group of early AMD model), L.C (control group of late AMD model), E.A (early AMD, L.A (late AMD), (Scale bar: 100 µm).

Figure 14: Graph of the average intensity of RPE65 protein expression.

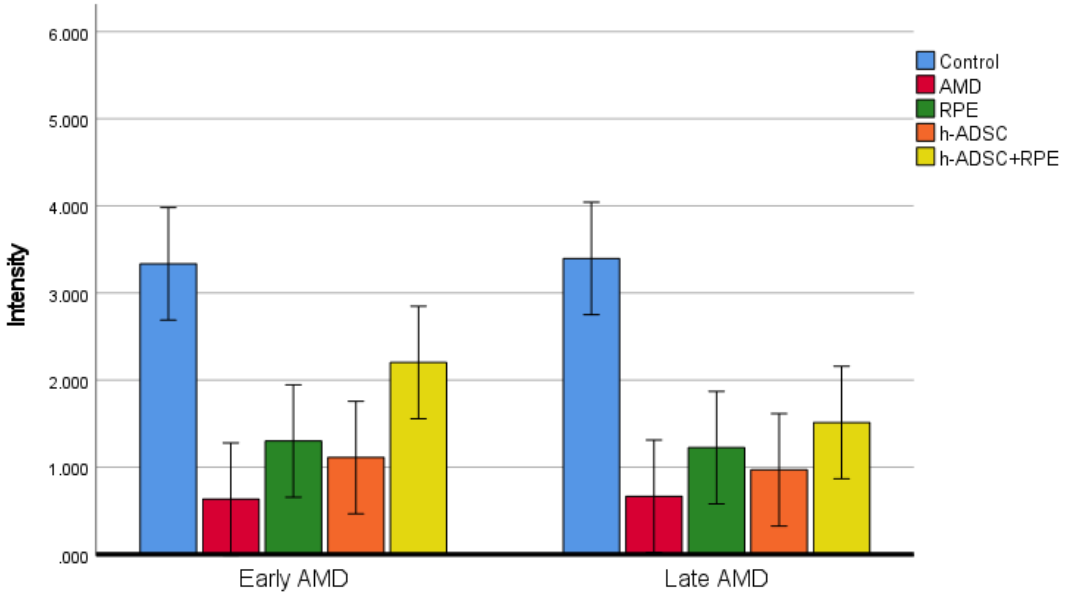

Illustration of the average intensity of RPE65 protein expression by the retinal pigment epithelium layer in two Early and Late AMD models and 5 groups of each model. The results showed that the effect of the treatment groups on the intensity was significant ($P < 0.001$), whereas the main effect of group and the interaction effect of phase × treatment on the intensity were not significant ($P > 0.05$). In the early AMD model, there was a significant difference between the mean intensity in the Control group and the other groups except h-ADSC + RPE ($P < 0.01$). In the late AMD model, the difference in the mean intensity was significant between the Control group and the other groups ($P < 0.05$), whereas there was no statistical difference between the other groups.

ONL; outer nuclear layer, PL; photoreceptors layer.

Figure 15: Qualitative observations of treatment samples of early and late models.

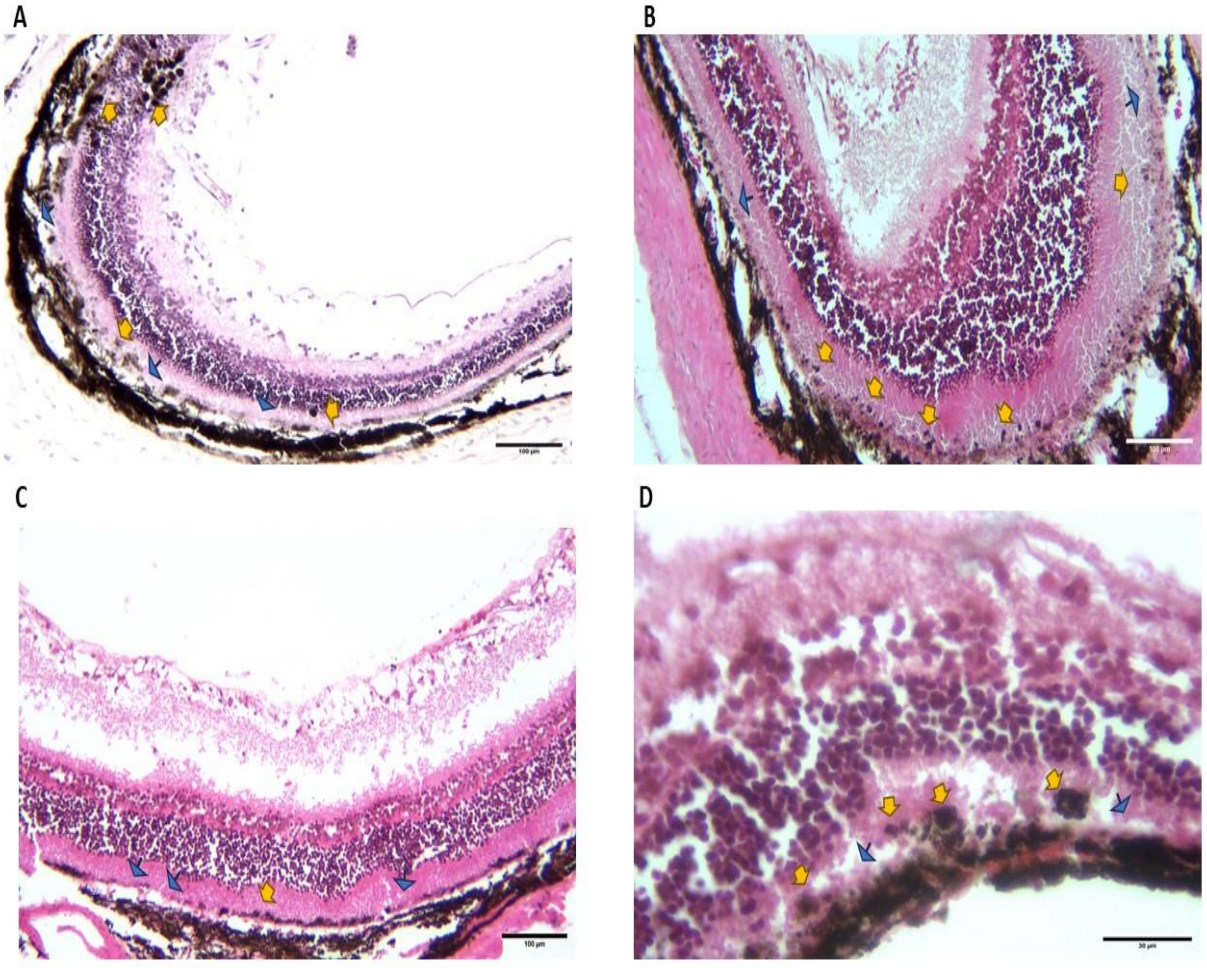

Microscopic view of the retina following therapeutic intervention. Samples with H&E dye showed that most retinal layers after treatment were relatively regular and close to normal, and the layered arrangement was largely preserved. However, the RPE was not completely regenerated. A- D: some areas showed focal destruction and cell loss (arrow blue). Pigment irregularity, pigment dispersion, and localized aggregations (arrow yellow) were also observed in parts of the RPE. These changes indicate that although repair of the neural retina structure was largely successful, RPE regeneration remained incomplete and was accompanied by localized abnormalities (Scale bar: 100 µm).